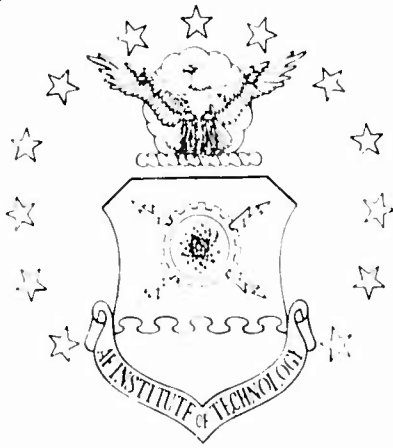


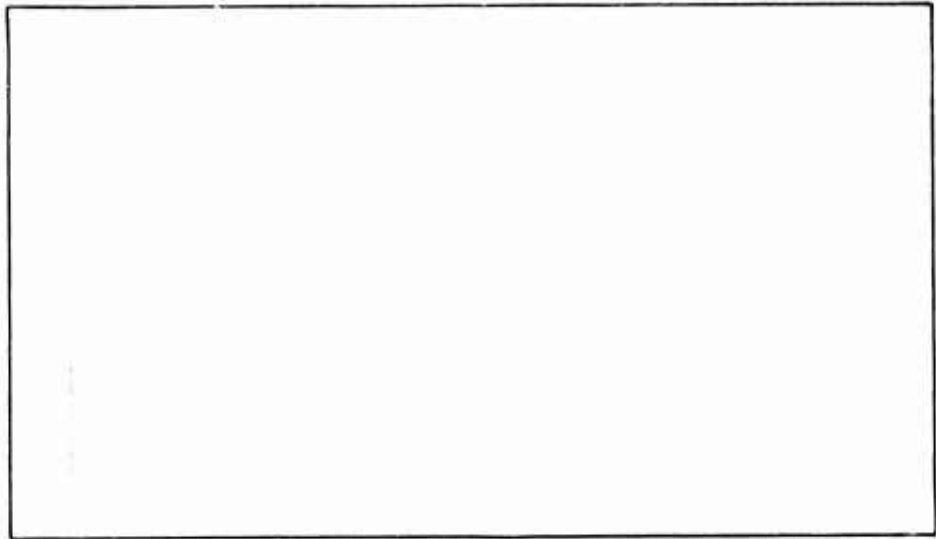
CLEARINGHOUSE FOR FEDERAL SCIENTIFIC AND TECHNICAL INFORMATION			
Hardcopy	Microfiche		
\$3.00	\$0.25	80	pp us
ARCHIVE COPY			

Copy 1

AIR FORCE INSTITUTE OF TECHNOLOGY



AIR UNIVERSITY
UNITED STATES AIR FORCE



SCHOOL OF ENGINEERING

WRIGHT-PATTERSON AIR FORCE BASE, OHIO

GAM/ME/66A-3

THIN-FILM
HEAT TRANSFER GAGES

GAM/ME/66A-3
John William Frye, Jr.
Captain USAF

GAM/ME/66A-3

THIN-FILM HEAT TRANSFER GAGES

THESIS

Presented to the Faculty of the School of Engineering of
the Air Force Institute of Technology
Air University
in Partial Fulfillment of the
Requirements for the Degree of
Master of Science

by

John William Frye, Jr. B.S.M.E.

Captain

USAF

Graduate Aerospace-Mechanical Engineering

March 1966

Preface

This report represents my attempt to provide the AFIT Resident School of Engineering with a facility to measure heat transfer in quasi-steady shock tube flow. To this end thin-film heat transfer gages were designed, constructed, installed, and tested in the AFIT 4 by 8 in. shock tube.

In the analysis of the heat transfer data (obtained using the thin-film gages) an assumption was made regarding the theoretical data given by Weatherston, et al. (Ref. 32). The assumption involved dividing the quantity B_L (laminar boundary layer heat transfer parameter) by $P^{\frac{1}{2}}$ (pressure behind the shock wave) and thereby obtaining a parameter that plots as a single curve for all pressures. Without more accurate B_L data, I cannot be sure that my assumption is completely valid, even though the existing evidence is overwhelmingly in favor of this procedure. In any case, I accept full responsibility for all the results due to this assumption, and all the other results of this study.

I would like to take this opportunity to express my appreciation to the following people: Professor Milton Franke, my thesis advisor, for his assistance, guidance, and encouragement; Dr. Muller and Dr. Grimm, ARL, and Capt. Robert Bowman, Professor, for their guidance and counsel on thin-film gages; Capt (Dr.) Donald Merkl, ASD, for his friendship and assistance in the electric circuit analysis; Mr. Wyson, ARL Ceramics Lab., for his time and assistance with the Cavitron drill; Mr. Richard Brown, M.E. Lab., for his patient

GAM/ME/66A-3

assistance with the shock tube apparatus; and lastly my wife, who not only tolerated me during this undertaking, but who inspired me to do the very best I could.

Contents

Preface	ii
List of Figures	vi
List of Tables	vii
List of Symbols	viii
Abstract	x
I. Introduction	1
Purpose	1
Background	1
II. Theory	4
Heat Conduction in the Gage	4
Data Reduction Equations	7
Heat Transfer to the Shock Tube Side Wall ..	9
III. Equipment	11
Thin-Film Gages	11
Shock Tube	13
Instrumentation	13
IV. Procedure	16
Gage Construction	16
Gage Calibration	16
Gage Experimental Procedure	18
V. Results and Discussion	21
Thin-Film Gage Construction	21
Velocity Measurements	22
Heat Transfer Measurements	23
VI. Conclusions	31
VII. Recommendations	33
Bibliography	34
Appendix A: Gage Construction	37
Appendix B: Gage Calibration	42
Appendix C: Sample Calculations	47

GAM/ME/66A-3

Appendix D: Accuracy Analysis	52
Appendix E: Shock Tube Modifications	60
Appendix F: Commercial Apparatus	63
Appendix G: Control Panel Layout and Drawings of the Gage Mounting Components	65

List of Figures

Figure		Page
1	Heat Conduction Model	4
2	Gage Operating Circuit	8
3	A Typical Thin-Film Gage	11
4	Side Wall Gage Installation	12
5	Instrumentation	14
6	Schematic of the Gage Lead Attachment	17
7	Gage Calibration Circuit	18
8	A Typical Oscilloscope Trace Generated by a Thin-Film Gage	19
9	Effect of Diaphragm Pressure Ratio on Shock Mach Number in the AFIT 4 x 8 in. Shock Tube.	24
10a	Boundary Layer Development in Shock Coordinates	25
10b	Typical Temperature History of a Point on the Wall	25
11	The Effect of Shock Mach Number on Laminar Boundary Layer Heat Transfer	28
12	The Effect of Shock Mach Number on the Step in Wall Temperature Behind a Moving Shock Wave	29
B-1	A Typical Calibration Response Using a Fixed Carbon Resistor in Place of the Gage	43
B-2	A Typical Calibration Response Using a Thin- Film Gage	43
B-3	Converted Calibration Curve (ΔE vs t to ΔE vs t^2)	46
E-1	The High Pressure End of the AFIT 4 x 8 in. Shock Tube	61
E-2	The Modified Shock Tube Control Console	62
G-1	Heat Transfer Gage Control Panel	66
G-2	Gage Holder and Gage Blank	67

List of Figures

Figure		Page
G-3	Adaptor, Brass (Gage Holder to Shock Tube)	68

List of Tables

Table		Page
1	Thin-Film Gage Set III	21
D-1	Data Error Analysis	53

List of Symbols

Symbol	Quantity	Unit
A	Area	in. ² or ft ²
(A)	Ammeter	
B _L	Laminar boundary layer heat transfer parameter	B/ft ² sec ^{1/2}
B _T	Turbulent boundary layer heat transfer parameter	B/ft ² sec ^{0.2}
B' _L	q (t/P _{atm}) ^{1/2}	B/ft ² sec ^{1/2} atm ^{1/2}
C _p	Specific heat at constant pressure for air	B/lbm F
c	C _p for the thin-film gage	B/lbm F
E	Voltage as recorded on an Oscilloscope	volt
I	Current	amp
k	Thermal conductivity	B/hr ft F
K	Thermal diffusivity (k/ρC _p)	ft ² /hr
K ₁	K for the platinum film	ft ² /hr
K ₂	K for the quartz backing material	ft ² /hr
L	Thickness of the platinum film	in.
M _s	Shock wave Mach number	
P _a	Ambient pressure	in. Hg.
P ₀	Reference pressure (29.92)	in. Hg.
P ₁	Station pressure prior to shock wave arrival	in. Hg. or atm
P ₂	Station pressure after shock wave arrival	in. Hg. or atm
P ₄₁	Shock tube diaphragm pressure ratio	
q	Heat transfer rate per unit area	B/ft ² sec
R	Resistance	ohm

R_0	Room temperature resistance of thin-film gage	ohm
R_2	Bridge resistor (in series with R_0)	ohm
T	Temperature	F or R
T_1	Temperature in the platinum film	F or R
T_2	Temperature in the quartz backing material.	F or R
T_r	Recovery temperature of the flow behind the shock wave	F or R
t	Time	sec
U_2	Velocity of the flow behind the shock wave.	ft/sec
U_s	Weatherston, et al. notation for shock velocity	ft/sec
V_a	Speed of sound in air	ft/sec
V_b	Voltage across bridge	volt
V_s	Shock wave speed	ft/sec
x	Dummy variable of integration	
α	Thin-film gage temperature sensitivity..	ohm/ohm F
β	Thin-film gage bulk heat transfer parameter $(\pi k \rho c)^{1/2} / 2\alpha$	B/ft ² sec ^{1/2}
ρ	Density	lbm/ft ³
μ in.	Microinch	in.x10 ⁻⁶
μ sec	Microsecond	sec x 10 ⁻⁶

Subscripts

w	Referring to properties evaluated at the wall surface
w _g	Gas properties at the wall surface

Abstract

An extensive literature survey on thin-film heat transfer gages was accomplished and pertinent references are listed. Methods and techniques for fabricating, calibrating, and using thin-film gages are discussed. Thin-film gages were fabricated using liquid platinum paint applied to a quartz backing material, and were calibrated using the electrical single pulse method. Rates of heat transfer were determined for a station on the wall of a shock tube for the laminar boundary layer flow condition immediately after shock wave passage for shock Mach numbers between 1.15 and 2.50. The variation of the wall surface temperature with time associated with shock wave passage was also determined. The results were correlated with theoretically predicted values and with the experimental results given by Hartunian and Weatherston.

The thin-film gages constructed for this study had determined values of $\frac{1}{2}(\pi\rho kc)^{\frac{1}{2}}$ of $0.067 \pm 0.005 \text{ B/ft}^2\text{F sec}^{\frac{1}{2}}$, and measured values for sensitivity of resistance to temperature ranging from 0.000905 to 0.001375 ohm/ohm F.

Thin-Film Heat Transfer Gages

I. Introduction

Purpose

The purpose of this study was fourfold: Survey the literature on thin-film heat transfer gages; design, fabricate and calibrate a set of these gages; design and fabricate the electric circuits required to calibrate and operate the gages; and demonstrate the use of the gages by making representative heat-transfer measurements.

Background

Although the shock tube has been in existence for about sixty-seven years, it has been since World War II that widespread use of the shock tube has become commonplace at universities and in industry. The use of the shock tube grew slowly at first, and the slow growth was due (at least in part) to the lack of adequate instrumentation. Instruments normally considered ideal for steady-state gasdynamic studies were found to be grossly inadequate for use in shock tubes. This inadequacy was due to the response times of the instruments which were relatively long when compared with the shock tube flow time. The advancements of piezoelectric pressure gages and high speed photography during World War II greatly accelerated the development of fast response shock tube instrumentation. The advances in fast response instruments, combined with increased research into supersonic flow phenomenon following World War II, promoted

a surge of studies using the shock tube. In more recent years the shock tube has been established as a research tool for studies in high-temperature kinetics (Ref. 3:8) and heat transfer phenomenon (Ref. 14:1).

In 1956, Vidal (Ref. 30) investigated and developed a new type of rapid response gage: the thin-film resistance thermometer. This new gage made heat-transfer measurements in shock tubes both possible and practical. The gages investigated by Vidal were very sensitive to temperature changes and had response times down to 0.05 μ sec, making them especially applicable for temperature change measurements in shock tubes. Due to the extremely fast response time, the gages were also well suited for use in the determination of shock wave velocity. Shock wave passage over the gages would generate a pulse due to the temperature change across the shock wave. By recording the time between two pulses, and knowing the distance involved, the velocity of the shock wave could be determined very accurately. In fact, some authors feel that the thin-film gage is the most accurate instrument available for determining shock wave velocities in shock tubes (Ref. 12:224). The use of the thin-film gage was effectively extended into the realm of ionized flows in 1959 by Marrone and Hartunian (Ref. 18). They electrically insulated the gage to prevent shorting by the ionized gas without appreciably affecting the gage sensitivity or response time.

Of all of the references found, not one author gave a complete detailed description of how to make a thin-film

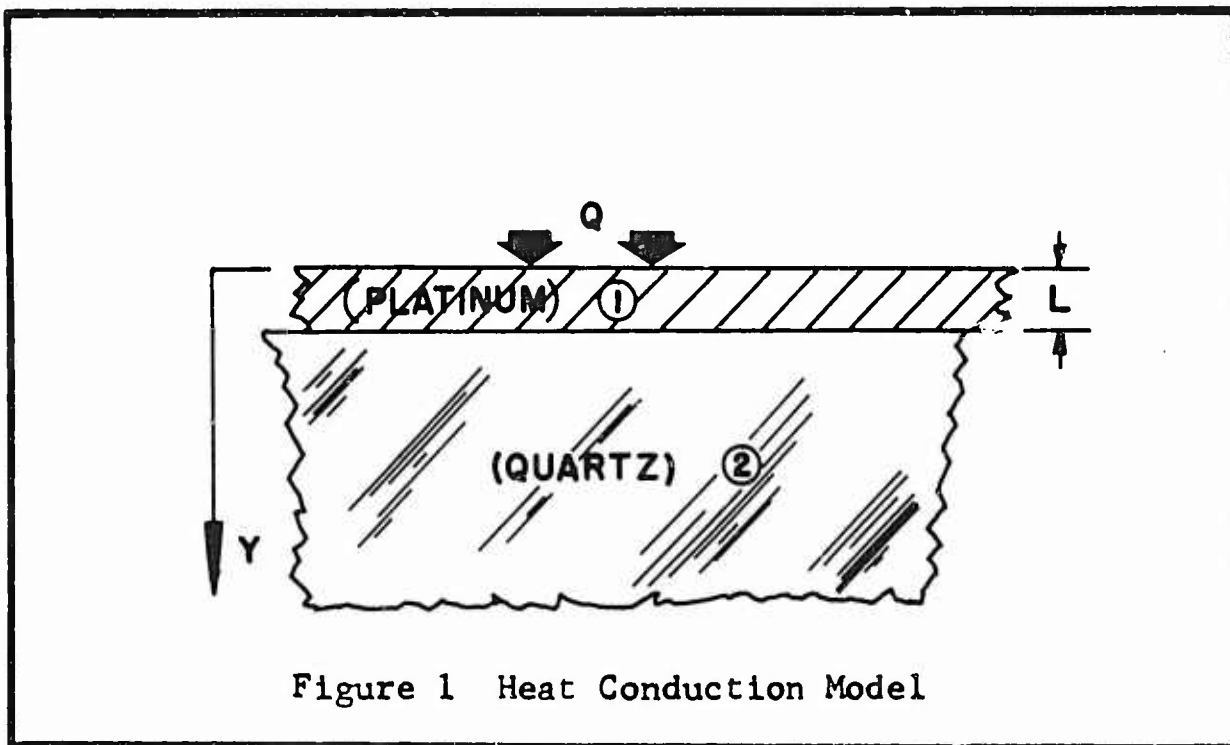
gage (except Ref. 20, which described the sputter method). Perhaps the details were omitted because of the outward simplicity of the process. In any case, the simplicity of the process is misleading because the successful and accurate fabrication of a thin-film gage requires patience, practice, and strict adherence to a few simple, but required, procedural steps. For this reason, a detailed description of the process used to fabricate the thin-film gages used in this study is included as Appendix A.

II. Theory

The purpose of the first part of this section is to outline the heat conduction theory applicable to the thin-film gage, and to outline the equations required to reduce the experimental data of this study to a form suitable for presentation and correlation. The second part of this section outlines the equations that were used to calculate theoretical values to correlate with the experimental results.

Heat Conduction in the Gage

A heat conduction model of the thin-film gage is shown in Fig. 1. The one-dimensional model is justified by the



following reasons: a typical platinum film (Fig. 1, region 1) is less than 10 μ in. thick, while it is 1/16 in. wide and 5/16 in. long. Therefore, roughly 10,000 times as much area is exposed by the surface perpendicular to the heat flow as

is exposed by the edges. Consequently, the heat flow perpendicular to the film should be at least 3 orders of magnitude greater than the lateral heat flow through the film. In addition, the only lateral temperature gradients that exist are extremely small, being caused by the finite traverse time of the shock wave across the gage surface. Therefore, the lateral heat flow will be neglected. The quartz backing (Fig. 1, region 2) is treated as an infinitely thick slab. This assumption is justified by the very short test times associated with shock tubes. Vidal (Ref. 30:7) justifies using the infinite slab assumption for region 2 based on a 1/16 in. thick slab; for this study the material in region 2 was quartz, 1/8 in. thick.

The basic equation governing unsteady heat conduction in region 1 is

$$\frac{\partial T_1}{\partial t} = K_1 \frac{\partial^2 T_1}{\partial y^2} \quad (1)$$

And the similar equation for region 2 is

$$\frac{\partial T_2}{\partial t} = K_2 \frac{\partial^2 T_2}{\partial y^2} \quad (2)$$

The exact solution to the above system of equations, with appropriate boundary conditions, involves the use of Laplace transforms and error functions and is given by Vidal (Ref. 30:7). The exact two-body solution is a very complicated

function and is not suitable for manual calculations. However, by making further assumptions the solution to Eqs. 1 and 2 is greatly simplified: first, the thermal conductivity of region 1 is taken to be very much greater than region 2, which is justified since region 1 is platinum, and region 2 is quartz. Secondly, the time interval of interest is large compared to L^2/K_1 . These two assumptions, combined with the previous 1-D assumption, show that the surface temperature and the mean temperature of the thin film are essentially the same. The exact solution for the surface temperature of a homogeneous body composed only of material 2 is

$$T(t) = \frac{1}{(\pi k \rho c)^{\frac{1}{2}}} \int_0^t \frac{q(x)}{(t-x)^{\frac{1}{2}}} dx \quad (\text{Ref. 30:20}) \quad (3)$$

For the simple case of a constant rate of heat transfer Eq. 3 integrates to

$$T(t) = 2q \frac{t^{\frac{1}{2}}}{(\pi k \rho c)^{\frac{1}{2}}} + T(0) \quad (4)$$

Vidal rigorously developed and compared the results of the homogeneous body solution, a first order approximation solution, and the exact two-body solution (Ref. 30:14). The homogeneous body solution differs by less than 3 percent from the exact solution if the time duration is greater than 100 μsec and the thickness of the film is less than 10 μin . The thicknesses of the gages constructed for this study were

assumed to be less than 7 μ in. based on information given by Vidal (Ref. 30:30) and Weatherston, et al. (Ref. 32:49). The test times for this study were all in excess of 100 μ sec. Therefore, rewriting Eq. 4 in terms of q and ΔT yields

$$q(\text{const}) = \frac{(\pi k \rho c)^{\frac{1}{2}}}{2} \frac{\Delta T(t)}{t^{\frac{1}{2}}} \quad (5)$$

If q is not constant Eq. 3 can be inverted and integrated by parts to yield: (Ref. 31:10)

$$q(t) = \frac{(\pi k \rho c)^{\frac{1}{2}}}{2} \left[\frac{\Delta T(t)}{t^{\frac{1}{2}}} + \frac{1}{\pi t^{\frac{1}{2}}} \int_0^t \frac{x^{\frac{1}{2}} \Delta T(t) - t^{\frac{1}{2}} \Delta T(x)}{(t-x)^{3/2}} dx \right] \quad (\text{Ref. 31:10}) \quad (6)$$

Data Reduction Equations

Referring to the gage operating circuit (Fig. 2) and considering that $\Delta R/R_0$ and $\Delta I/I_0$ are on the order of 1 percent or less, the change in voltage across the bridge is very closely approximated by

$$\Delta E = \frac{\Delta R R_2 V_b}{(R_0 + R_2)^2} \quad (7)$$

Again referring to Fig. 2, the steady state current through the gage is

$$I_0 = \frac{V_b}{R_0 + R_2} \quad (8)$$

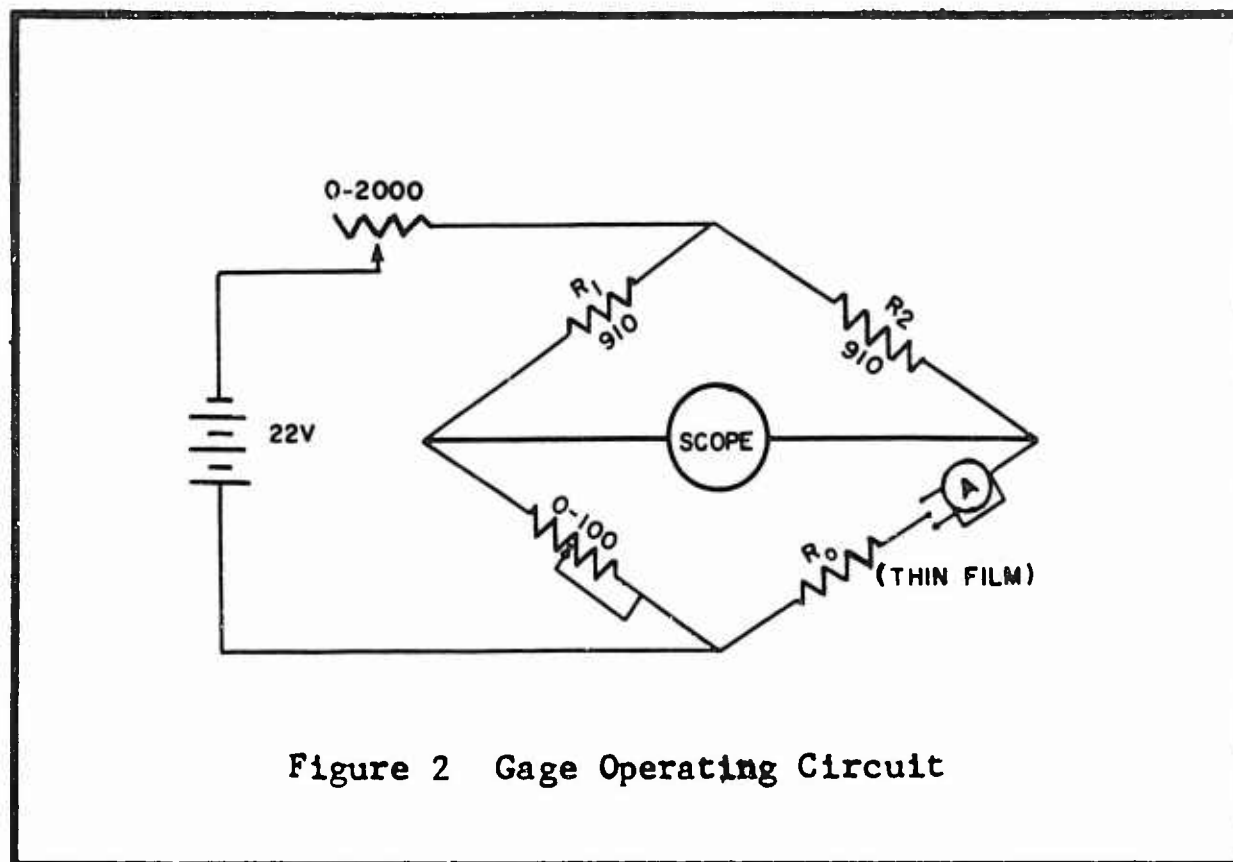


Figure 2 Gage Operating Circuit

To relate ΔR with ΔT , the resistance of each gage was measured at 32F and at room temperature, and a linear relationship between resistance and temperature was assumed:

$$\Delta R = \alpha \Delta T R_0 \tag{9}$$

To assume that a linear relationship holds over the limited range of gage temperatures encountered in this study (80 ± 10 F), agrees with all of the references listed in the Bibliography that treat this subject. To relate the gage temperature change to the change in voltage across the bridge, Eqs. 7, 8 and 9 are combined to yield

$$\Delta T = \frac{R_0 + R_2}{\alpha R_2 R_0 I_0} \Delta E \tag{10}$$

Rewriting Eq. 4 in terms of ΔT yields

$$\Delta T = 2q \frac{t^{\frac{1}{2}}}{(\pi k \rho c)^{\frac{1}{2}}} \quad (11)$$

An expression relating the voltage change across the bridge to a constant heat flux through the thin-film gage is obtained by equating Eqs. 10 and 11 and rearranging:

$$q(\text{const}) = \frac{(\pi k \rho c)^{\frac{1}{2}}}{2} \left[\frac{R_0 + R_2}{R_2 R_0 I_0} \right] \frac{\Delta E(t)}{t^{\frac{1}{2}}} \quad (12)$$

Notice that the only difference between Eqs. 5 and 12 is the insertion of a constant and the substitution of ΔE for ΔT . If the heat flux is not a constant, the relationship between q and ΔE is obtained by combining Eqs. 6 and 10:

$$q(t) = \frac{(\pi k \rho c)^{\frac{1}{2}}}{2\alpha} \left[\frac{R_0 + R_2}{R_2 R_0 I_0} \right] \left[\frac{\Delta E(t)}{t^{\frac{1}{2}}} + \frac{1}{\pi t^{\frac{1}{2}}} \int_0^t \frac{x^{\frac{1}{2}} \Delta E(t) - t^{\frac{1}{2}} \Delta E(x)}{(t-x)^{3/2}} dx \right] \quad (13)$$

Heat Transfer to the Shock Tube Side Wall

The theoretical rate of heat transfer from the quasi-steady gas flow behind a moving shock wave to the shock tube side wall is given by Weatherston (Ref. 32:40) and by Hartunian (Ref. 14:14). The theoretical values for the rate of heat transfer through a laminar boundary layer were computed for this study using the relation

$$q_L = B_L t^{-\frac{1}{2}} \quad (\text{Ref. 32:44}) \quad (14)$$

GAM/ME/66A-3

Similarly, the theoretical heat transfer rate through a turbulent boundary layer was shown to be

$$q_T = B_T t^{-0.2} \quad (\text{Ref. 32:48}) \quad (15)$$

The terms B_L and B_T are functions of the initial shock tube conditions and the shock wave strength. B_L and B_T were developed, computed, and plotted by Weatherston, et al. (Ref. 32:118). Although the values for B_L used in this study were taken directly from Weatherston, et al., the complete equation for B_L is repeated here for reference:

$$B_L = (T_r - T_w) \left\{ \frac{1}{\pi} (k^p C_p)_{wg} \left[1 - (2^{\frac{1}{2}} - 1) \frac{U_2}{U_s} \right] \right\}^{\frac{1}{2}} \quad (16)$$

(Ref. 32:118)

III. Equipment

All of the equipment used in this study is commercially available, except the thin-film gages and the related gage electrical circuits. The major specifications for the commercial equipment are given in Appendix F and will not be described in detail.

Thin-Film Gages

A photograph of a typical gage and gage holder is shown in Fig. 3. The gage itself consists of a thin film of platinum fired on a 1/2-in. diameter disk of polished quartz.

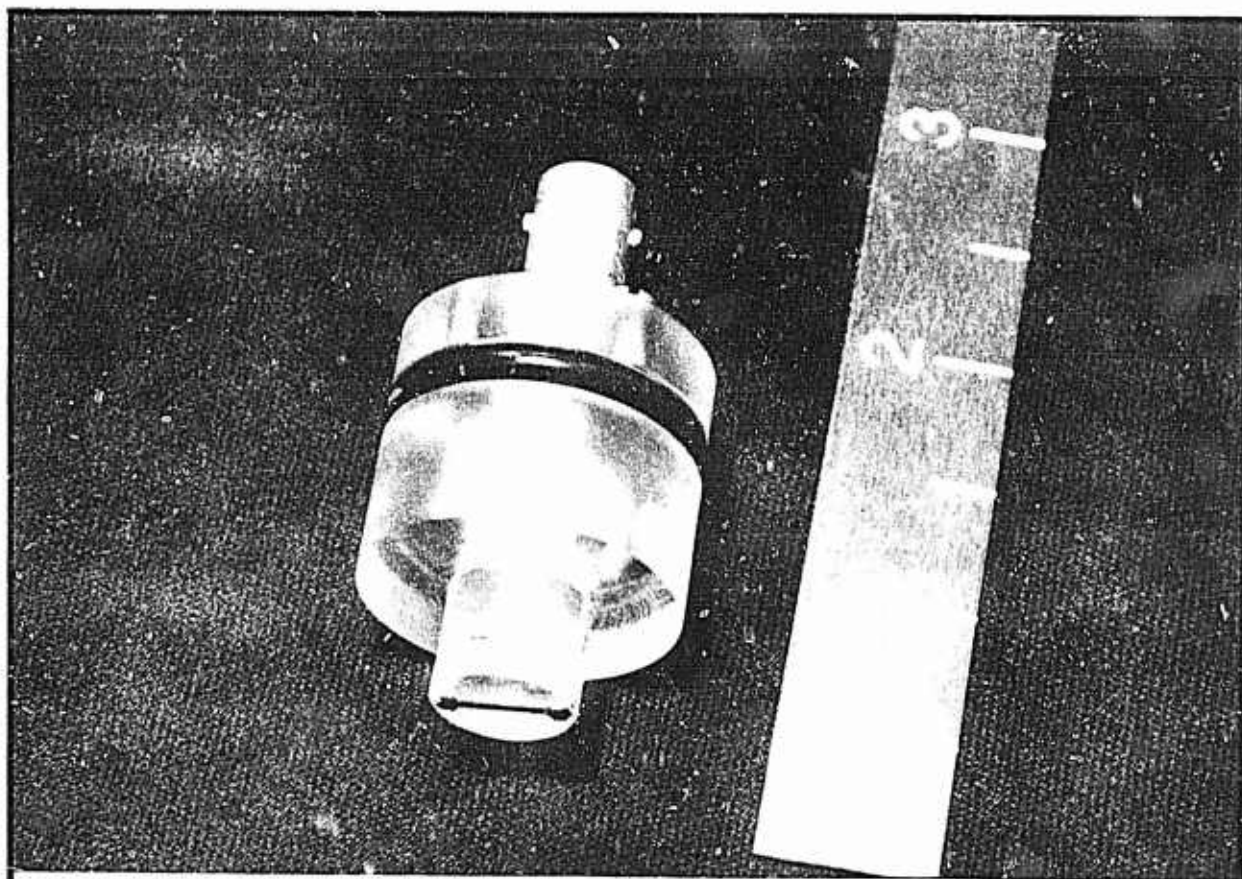
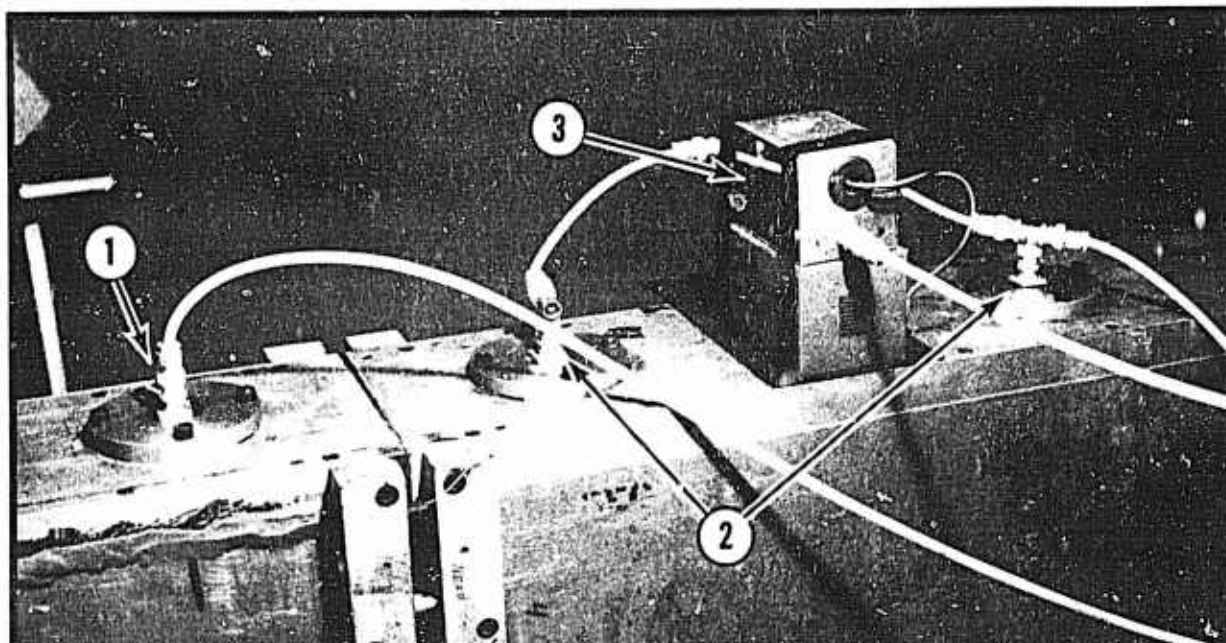


Figure 3 A Typical Thin-Film Gage
(Mounted on Holder)

Details of the materials and the method used to fabricate these gages are given in Appendix A. A drawing of the gage holder is given in Appendix G. The typical gage resistance was about 40 ohms. The dimensions of a typical film were approximately 0.04 in. wide and 0.3 in. long. Although the film thickness was not measured, Vidal (Ref. 30:30) states that the film thickness for the 05-X platinum is on the order of 10^{-6} in. when painted and fixed on glass. A complete list of the gages with their respective characteristics is given in Table 1 of Section V. Gages #5 and #7 were used to generate the start and stop pulses for the shock wave timer, and gage #4 was used to obtain the temperature change and heat transfer data. The side-wall gage installation used for this study is illustrated in Fig. 4.



- 1 Heat Transfer Gage
- 2 Timer Trigger Gages
- 3 1000X Amplifier

Figure 4 Side-Wall Gage Installation

Shock Tube

The AFIT shock tube is described in detail by Egan and Foster (Ref. 8:2) and will be only briefly described here. The basic shock tube has a constant 4 x 8 in. rectangular cross section. The length of the shock tube and test section configuration are variable. For this study the constant area test section was used and the shock tube length was set at 20 ft. The data for heat transfer through the boundary layer was taken at a station approximately 12.3 ft. from the shock tube diaphragm (Fig. 4).

A change was also made in the shock tube firing apparatus. An electrical valve in the firing mechanism was replaced by a manual valve because the electrical valve generated an excessive amount of electrical noise in the gage output. This change as well as a few other simple modifications are described in Appendix E.

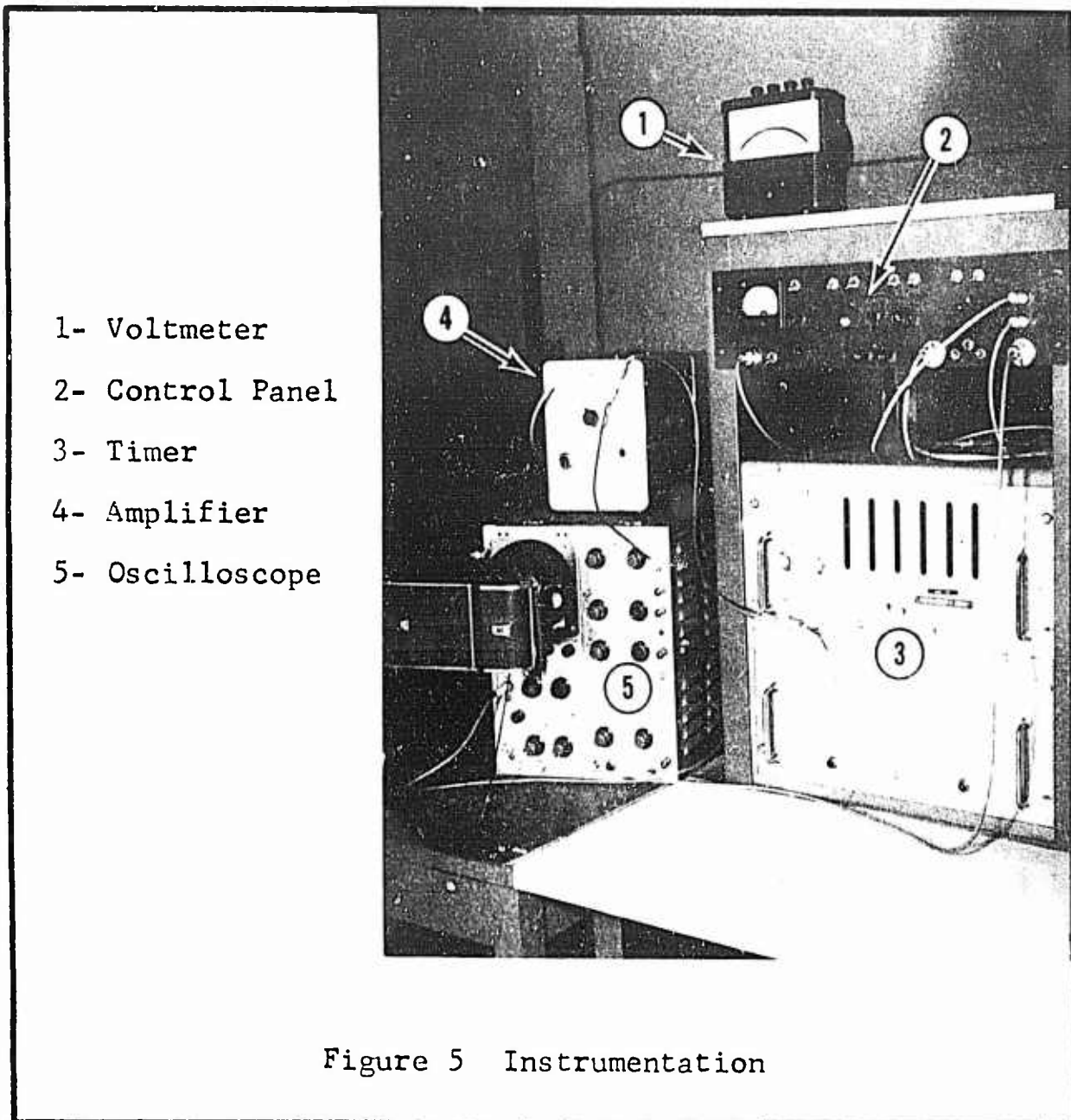
Instrumentation

An overall view of the recording instrumentation is shown in Fig. 5. The heat transfer data and the shock wave speed data were simultaneously recorded using this apparatus. The same instrumentation was used to record the data for heat transfer, gage calibration, and shock wave velocity.

The control panel (Fig. 5) served to house the operating circuit and the calibration circuit, and to provide a centralized location for cable connections. An enlarged view of the control panel is given in Appendix G.

A time interval meter (Fig. 5) was used to record the

elapsed time between the pulses generated by two thin-film gages mounted one ft apart on the shock tube wall (Fig. 4).



An oscilloscope (Fig. 5) was used to display the unbalance of the operating bridge (Fig. 2), or the unbalance of the calibrating bridge (Fig. 7). This instrument combined with a Polaroid camera provided a record of the applicable circuit response. A voltmeter (Fig. 5) was used to measure all steady state voltages.

GAM/ME/66A-3

The thin-film gage triggering pulses were considerably amplified to achieve reliable operation of the time interval meter. The voltage change generated by the gages upon shock wave passage were amplified 1000X by a solid state, locally fabricated, 22 volt, pulse amplifier (Fig. 4). This amplified pulse was then passed through a second amplifier (Fig. 5) and amplified by an additional 20X. The heat transfer signals were not amplified.

A resistance bridge coupled with a galvanometer was used to measure all resistances.

IV. Procedure

The procedure can logically be divided into three distinct parts: the procedure that was used in the construction of the thin-film gages, the procedure that was used to calibrate the gages, and the procedure that was used in the experimental application of the gages.

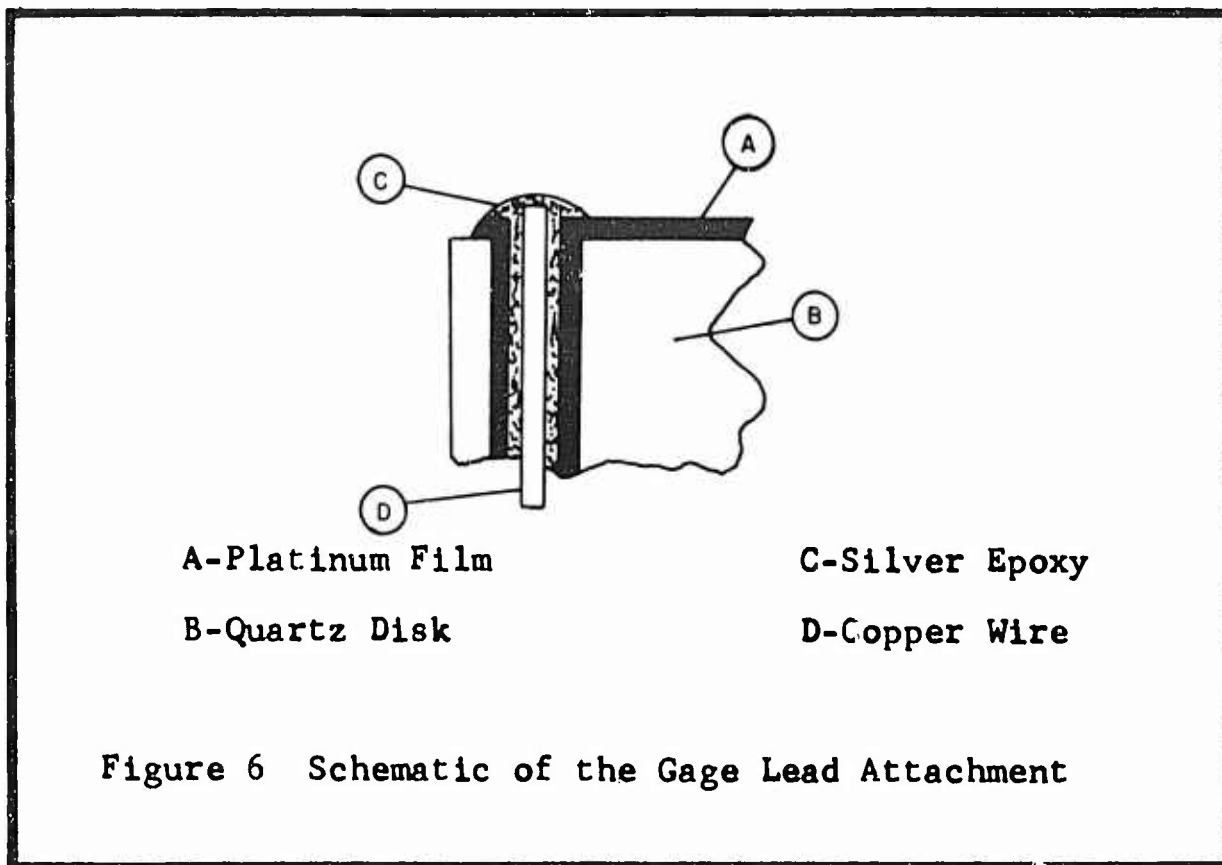
Gage Construction

A thin film of platinum paint was deposited, using a drawing pen, on a 1/2-in.-diameter quartz disk (Figs. 3 and G-2). The film was then baked on the quartz at 1300F for about 5 hrs. Copper lead wires were attached to the quartz and film using conducting epoxy to complete the electrical connection (Fig. 6). Although the success to failure ratio improved considerably with increased experience, the overall attrition rate (including practice gages, rejects, and accidental or intentional destruction) was approximately 80 percent. For a detailed description and analysis of each step in the gage construction process see Appendix A.

Gage Calibration

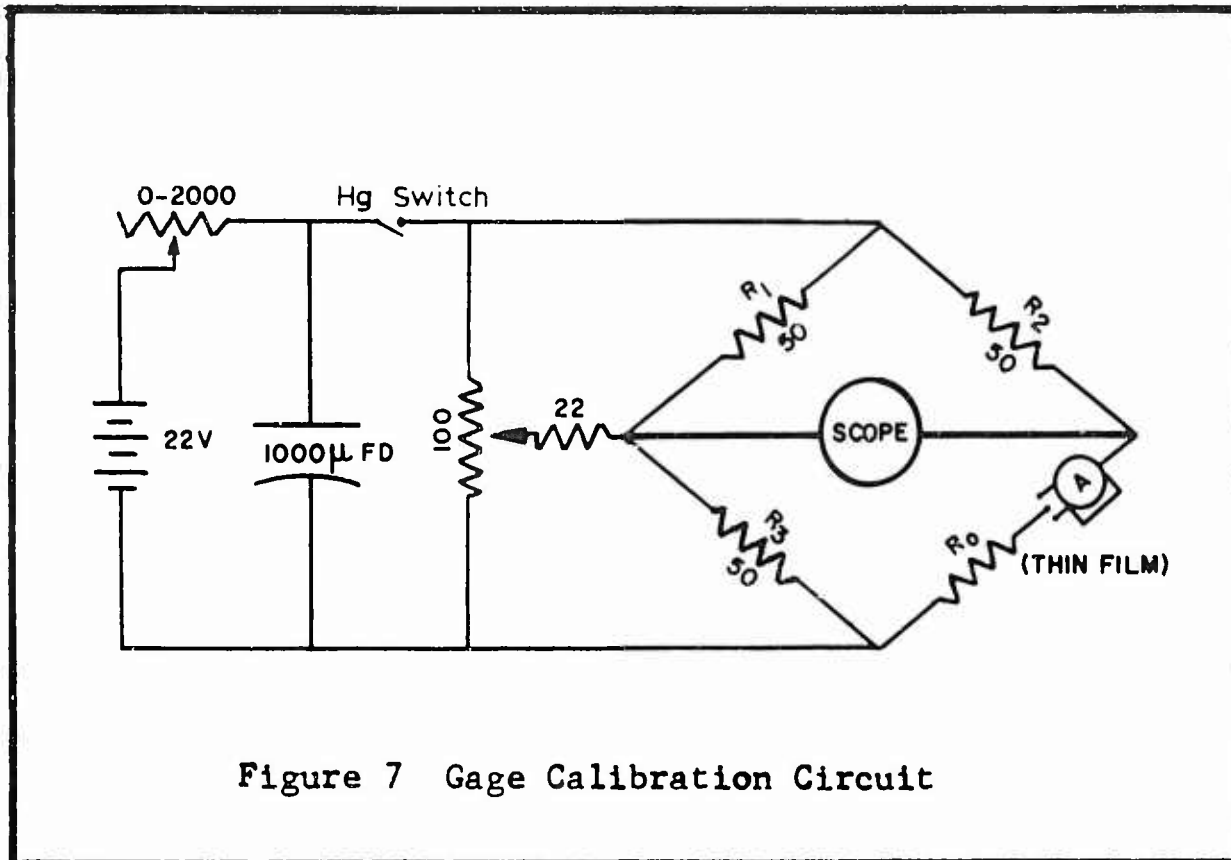
Currently there are two methods available for calibrating thin-film gages electrically. Both of these methods are appropriate and directly applicable to the gages used in this study. The double pulse method is the most accurate and is clearly described in the literature (Refs. 1, 16, and 25). However, the single pulse method offers the advantage of "in use" calibration. This feature permits

gage calibration without disturbing the gage or the experimental apparatus. The single pulse method also requires less calibration data. In any case, the single pulse method was used and yielded an accuracy and repeatability consistent with the other measured variables in this study.



Using the instrumentation (Fig. 5) and the calibration circuit (Fig. 7), a known electric charge was pulsed through the gage. The ohmic heating of the thin film caused the film to change resistance, which changed the balance of the bridge. The bridge unbalance, in turn, was presented on the oscilloscope and recorded on film. The film record was then evaluated using a traveling microscope. The bulk heat transfer parameter (β) of the gage was then computed from the known ohmic input and the gage response using Eq. B-4. A

more detailed analysis of the calibration circuit and technique is given in Appendix B.

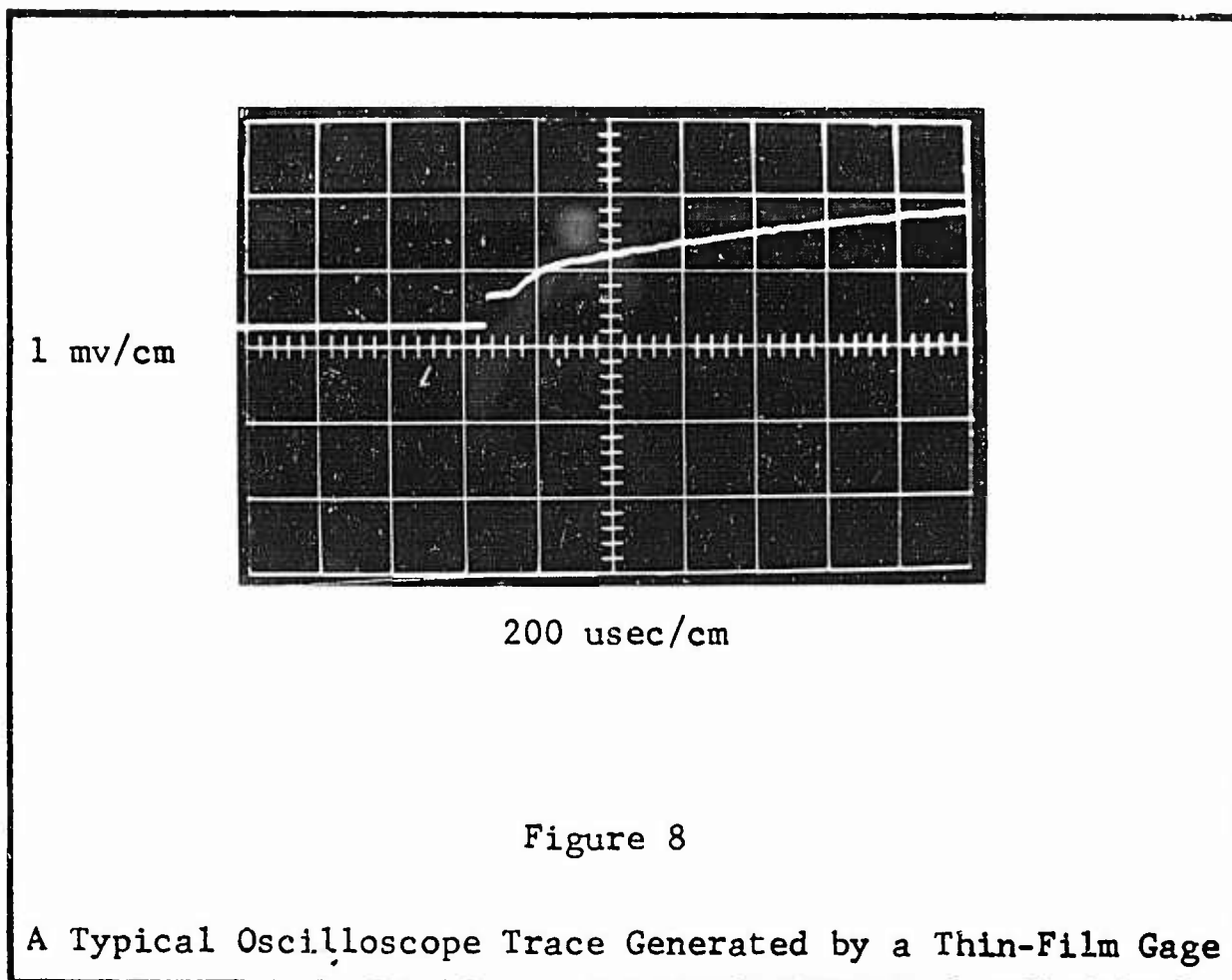


Gage Experimental Procedure

The objective of this portion of this study was to demonstrate the use of thin-film gages. To this end, the gages were used to determine shock wave velocities and wall heat transfer rates in a shock tube.

The shock wave velocity was determined by measuring the time required for the shock wave to travel across a known distance. The transit time was directly indicated in usec on a timer, which was started and stopped by two thin-film gages. The timing gages were mounted 1 ft apart in the shock tube side wall, and were located as close as possible to the heat transfer gage (Fig. 4).

A thin-film gage was used to indirectly measure the heat flux to the shock tube walls. The gage was mounted flush with the shock wall and downstream of the velocity gages. The heat transfer from the shock heated gas to the gage caused the gage to change temperature. The change in gage temperature caused a change in the gage resistance which, in turn, caused a change in the balance of the operating bridge (Fig. 2). The unbalance of the operating bridge was presented in millivolts on the oscilloscope and recorded on film (Fig. 8).



The photographs were evaluated using a traveling microscope. Using the gage response (as indicated on the photograph) and the known heat transfer coefficient of the gage, the rate of

GAM/ME/66A-3

heat transfer to the shock tube wall was calculated using the equations of Section II.

V. Results and DiscussionThin-Film Gage Construction

Characteristics of the gages constructed for this study are described in Table 1. Gage III-4 was used in the experimental determination of surface temperature change and the rate of heat transfer. Gages III-5 and III-7 were used to determine the shock wave velocity.

TABLE 1
Thin-Film Gage Set III

GAGE	R_o	α	β	AREA
#	ohms	ohm/ohm F	B/ft ² sec ^{1/2}	ft ² x 10 ⁴
1	63.76	0.000987	68.1	0.591
2	32.90	0.001758	39.2	0.834
3	47.69	0.000905	73.0	0.568
4	49.73	0.001065	66.3	0.663
5	35.52	0.001375	48.1	0.754
6	51.25	0.000927	71.3	0.702
7	33.45	0.000965	68.6	0.656

R_o depends on room temperature.

$$\beta = (\pi k \rho c)^{1/2} / 2\alpha$$

Vidal (Ref. 31:14), and all other reporting authors, give values of $\beta\alpha$ within 5 percent of 0.067 B/ft² F sec^{1/2}.

It is interesting to note that the handbook value for glass is $\beta\alpha = 0.066 \text{ B/ft}^2 \text{ F sec}^{\frac{1}{2}}$ (Ref. 31:14). Gage III-4, the gage used to take heat transfer data for this study, had a $\beta\alpha$ value of $0.0705 \text{ B/ft}^2 \text{ F sec}^{\frac{1}{2}}$. This value for $\beta\alpha$ deviates from Vidal's value by 5.23 percent. However, some loss of calibration accuracy was expected since the single pulse calibration method was used. The values of α compare favorably with the values given in numerous references; the value of α ranges from 0.0008 to 0.0020 ohms/ohm F, depending on the film width and thickness.

Velocity Measurements

The rise time for a thin-film gage is essentially the time it takes the shock wave to cross the gage. This being the case, it would be advantageous to construct very narrow gages for use in velocity detection circuits. The use of a special gage would be especially desirable if the detection probes were mounted close together. The gages used in the velocity circuit for this study were relatively wide (approximately 1/16 in.); however, they were selected to have similar widths to equalize their respective rise times. In any case, the probe distance involved (1 ft) was extremely large compared with the gage width, and the measured traverse time is believed to be accurate within 1 percent.

The theoretical curve for M_s vs P_{41} given by Egan and Foster (Ref. 8:Fig. 29) is shown with the experimental data taken in this study (Fig. 9). The deviation of the experimental data from the theoretical curve is attributed to the

fact that air is not a perfect gas. Specifically, a shock wave in a non-ideal gas produces a higher pressure and particle velocity ratio (across the wave) than it would in an ideal gas. This effect should become progressively worse at higher Mach numbers. In fact, Glass (Ref. 11:91) states that this effect will necessitate a 30 percent increase in P_{41} at $M_s = 4.3$ above the value predicted by the theoretical curve.

Heat Transfer Measurements

The surface temperature history was recorded in the form of a voltage/time trace. As was shown by Eq. 6, the surface temperature is directly related to the rate of heat transfer through the surface. The temperature histories on the shock tube side wall were recorded for shock wave Mach numbers between 1.16 and 2.50.

The side wall data not only demonstrates the capability of the gage to detect heat transfer through boundary layer flow, but illustrates the potential of the gage to indicate boundary layer transition. The development of the boundary layer in a shock tube is shown (in shock wave coordinates) by Fig. 10a.

All side wall data taken for this study had the characteristics shown in Fig. 10b except the very weak shock waves (less than $M_s = 1.25$). The very weak shocks simply caused a small step in the trace at shock wave passage (temperature steps as low as 0.24 F were recorded), but, for these low Mach numbers, the transition from laminar to turbulent

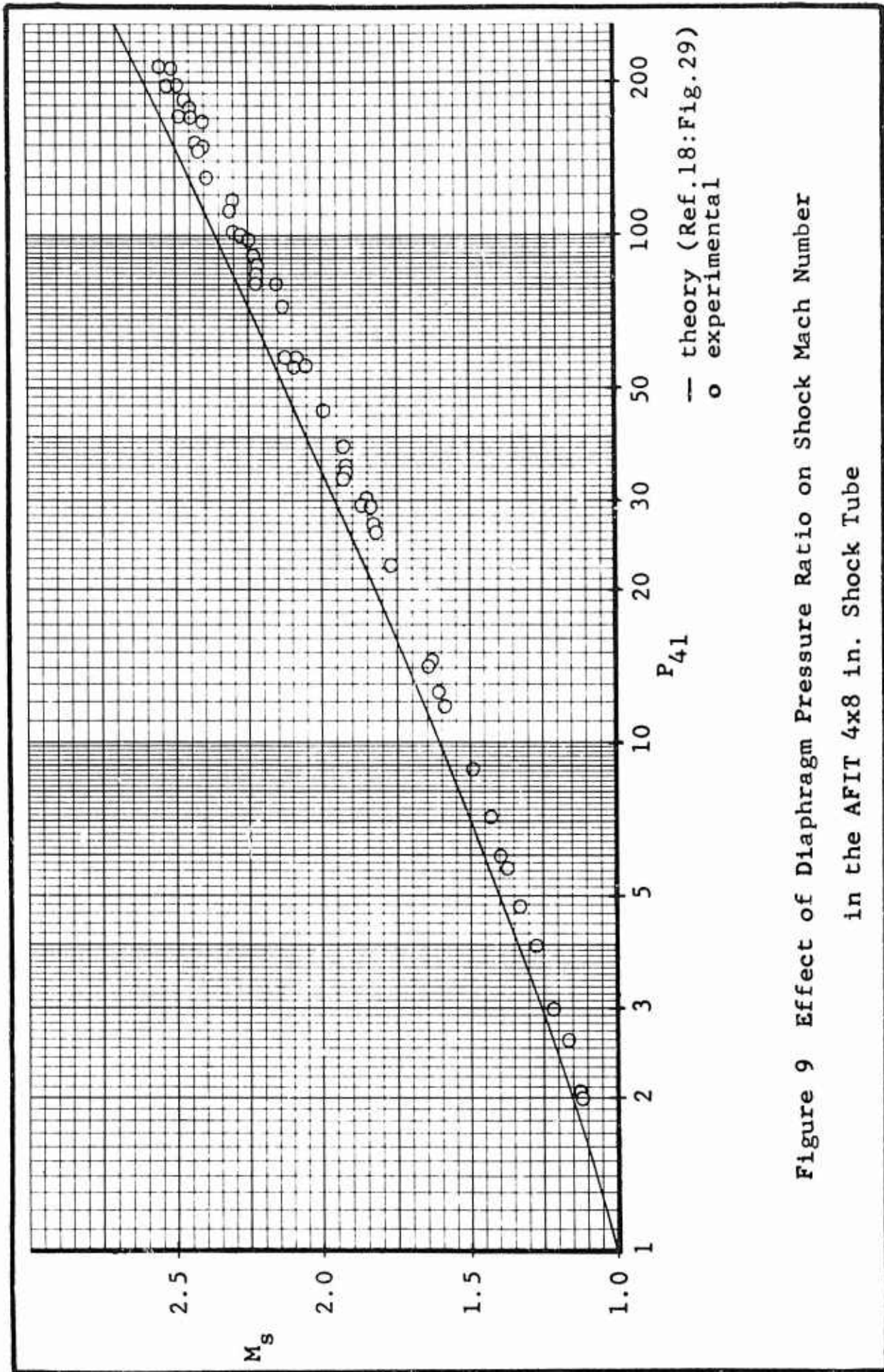


Figure 9 Effect of Diaphragm Pressure Ratio on Shock Mach Number
in the AFIT 4x8 in. Shock Tube

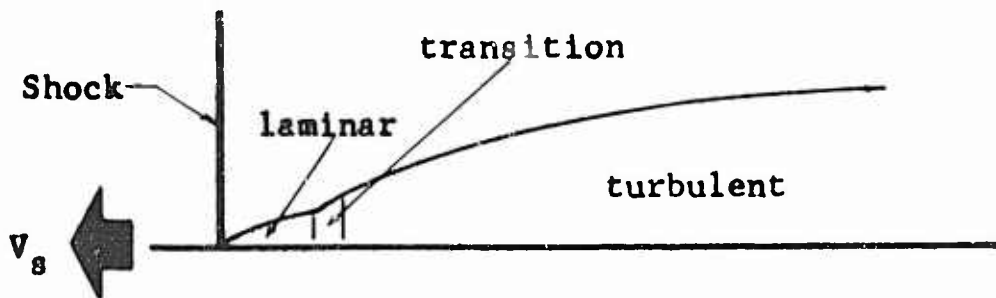


Figure 10a

Boundary Layer Development in Shock Coordinates
 (A gage which moves with the wall senses the temperature history shown in Fig. 10b)

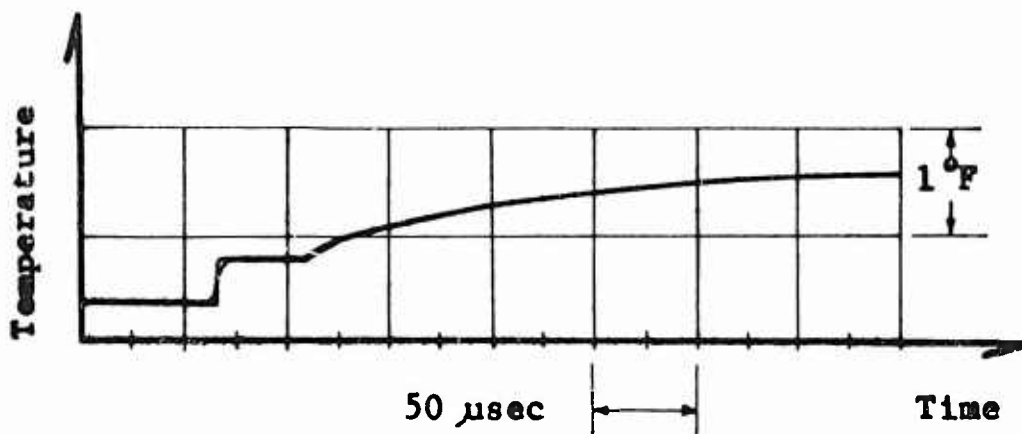


Figure 10b

Typical Temperature History of a Point on the Wall

Air to Air

Gage III-4

$M_s = 1.77$

$P_1 = 4.45 \text{ in. Hg.}$

$T_1 = 542 \text{ R}$

boundary layer was not distinguishable.

To achieve an overall impression of the laminar heat transfer data the value $q t^{\frac{1}{2}}$ was determined for all the side wall runs, and compared with B_L (Eq. 14). The parameter B_L is presented in graphical form by Weatherston, et al. (Ref. 32:114). An overall comparison of $q t^{\frac{1}{2}}$ with B_L proved to be very difficult because each run occurred at a different pressure which caused each experimental point to fall on a different curve. By analyzing the graphs given by Weatherston, et al. (Ref. 32:114), it was determined that all the curves of B_L could be reduced to a single curve. This was accomplished by dividing B_L by the root of the respective run pressure. The maximum distortion introduced by this manipulation was 10 percent. However, the deviation of 10 percent was found only at a few isolated points as compared to the majority of the points which (within the reading limits of the curves) agreed exactly. Therefore, a new parameter was defined as

$$B'_L = B_L/P^{\frac{1}{2}} = q (t/P)^{\frac{1}{2}} \quad (17)$$

or, in the complete form of Ref. 32:

$$B'_L = (T_r - T_w) \left\{ \frac{1}{\pi} (k P C_p)_{wg} \left[1 - (2^{\frac{1}{2}} - 1) \frac{U_2}{U_s} \right] \right\} \frac{1}{P^{\frac{1}{2}}} \quad (18)$$

The curve for B_L' using the graphs given by Weatherston, et al. (Ref. 32:118) is shown in Fig. 11 with all of the laminar boundary layer experimental data taken for this study. The fact that the experimental values are larger than the theoretical values is generally supported by the experimental data presented by Friedman and Fay (Ref. 10:1973), Scagnetti and Crabol (Ref. 22:29), and Taylor (Ref. 27:Fig. 7). Theoretically, the rate of heat transfer through a laminar boundary layer is a function of $t^{\frac{1}{2}}$; likewise, the one dimensional heat transfer rate to a body from a suddenly applied hot body is a function of $t^{\frac{1}{2}}$. Ideally, the temperature at the interface should jump to some intermediate temperature and remain constant as long as the boundary layer is laminar (Refs. 21:23, 30:37, 32:42). This is exactly the condition behind the shock wave in a shock tube, and is what the experimental data indicates (Fig. 10b).

The temperature change at the wall surface, as computed from experimental data using Eq. 10 (and again dividing by $P^{\frac{1}{2}}$ to eliminate the pressure dependence), is shown in Fig. 12 with the theoretical curve of Mirels (Ref. 32:117). This second comparison was made in order to introduce other experimental data that was available. As can be seen the experimental data tends to be less than the theoretical prediction by approximately 30 percent. However, the other experimental data, shown as a shaded area to avoid clutter, agrees fairly well with the data of this report.

The wall surface temperature, instead of being constant as it was for laminar boundary layer flow, increases with

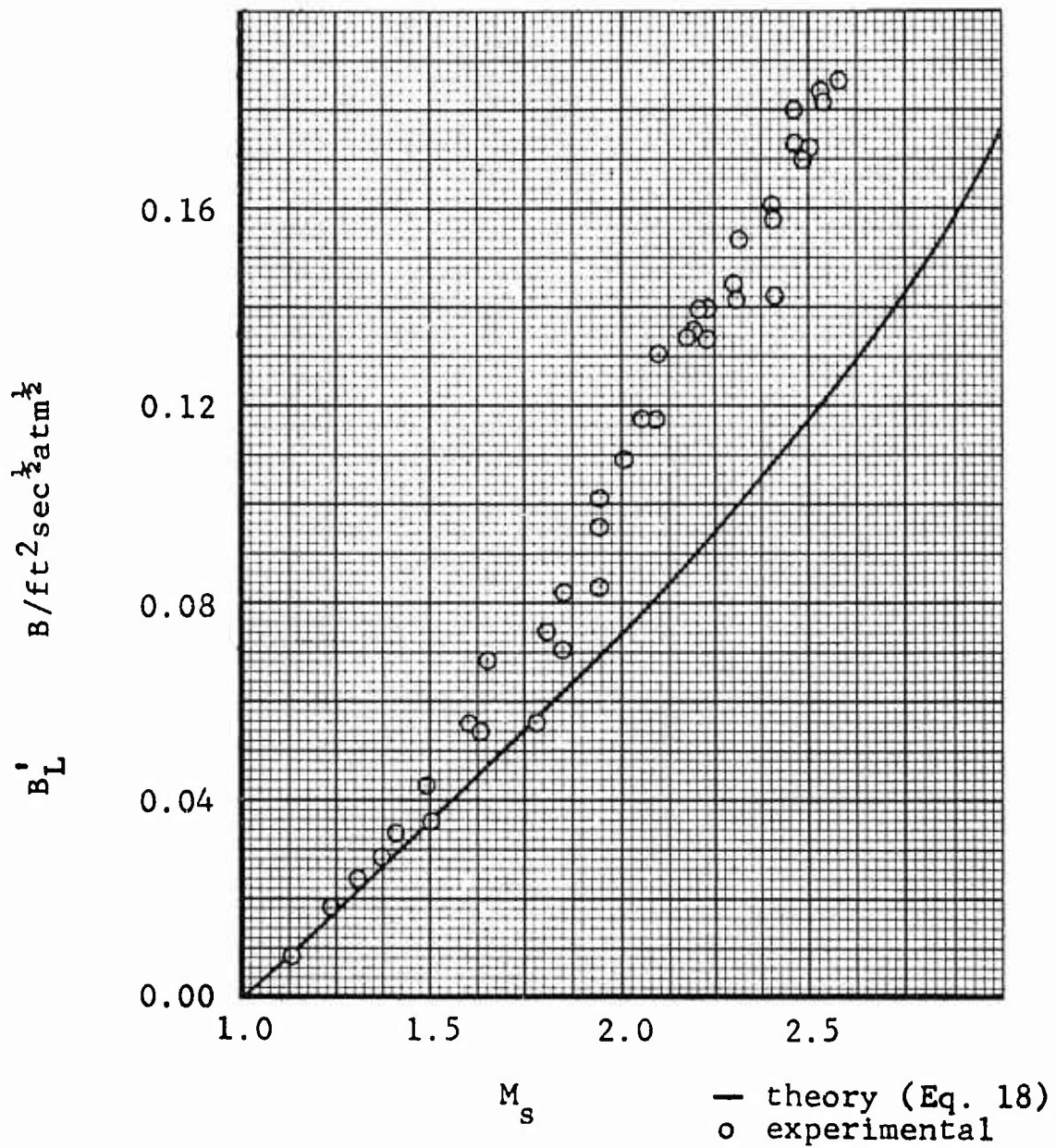


Figure 11
 The Effect of Shock Mach Number
 on
 Laminar Boundary Layer Heat Transfer

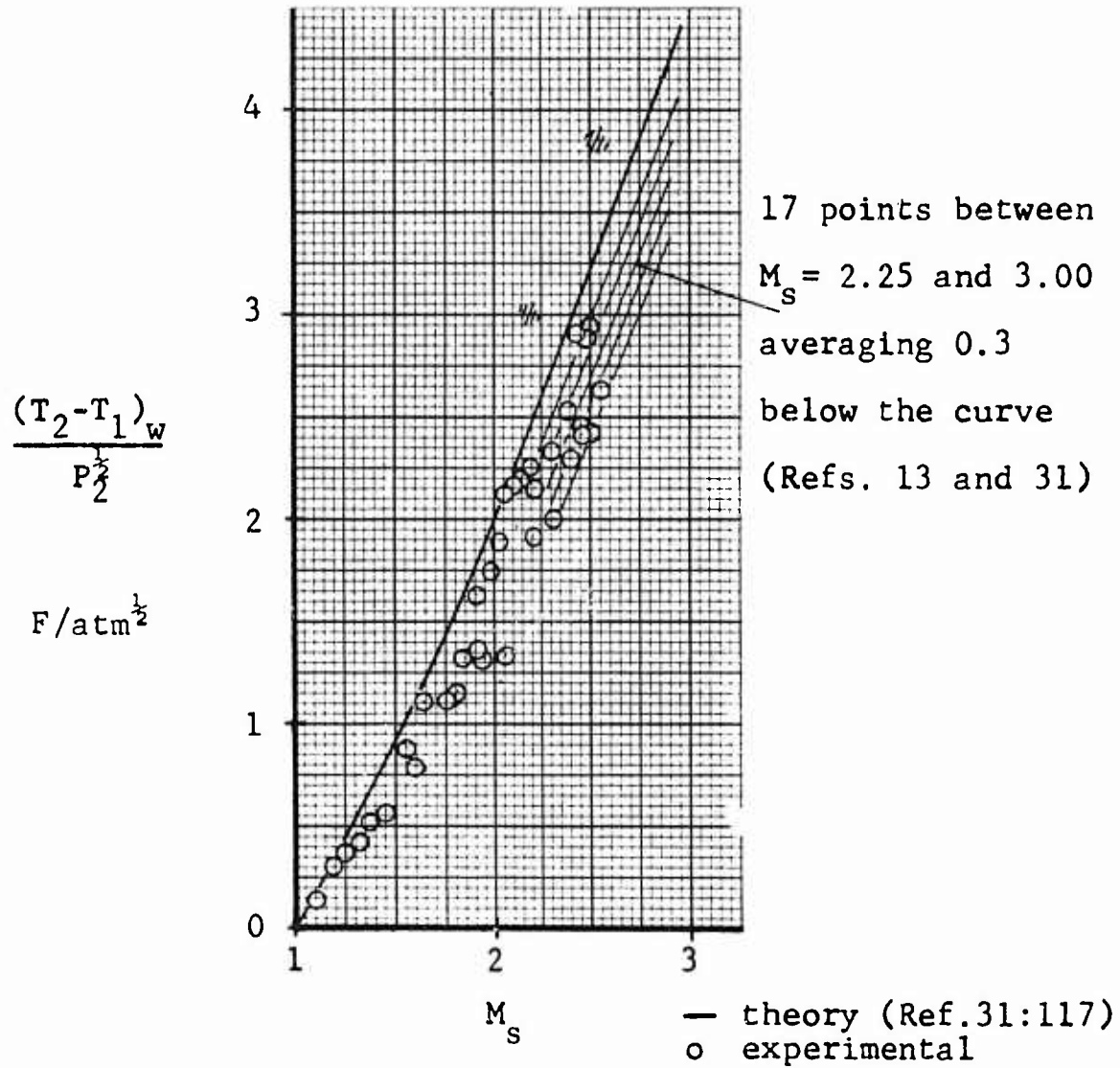


Figure 12

The Effect of Shock Mach Number

on

The Step in Wall Temperature Behind a Moving Shock Wave

time with turbulent boundary layer flow. Specifically, the wall surface temperature should rise initially as the three tenths power of time (Ref. 32:48). Also, there is a corresponding increase in heat transfer rate as shown by Eq. 15. The data of this study definitely agree qualitatively with these theoretical predictions. No attempt was made in this study to quantitatively reduce the turbulent boundary layer data which would require the evaluation of the integral in Eq. 13. A method that could be used to manually evaluate Eq. 13 for varying temperature at a given time is given in detail by Taylor (Ref. 27:16).

VI. Conclusions

1. With a reasonable amount of practice, thin-film heat transfer gages can be manually constructed using liquid platinum paint. Such gages appear to have a reasonably long life, depending on the nature of the application. After more than 100 runs, no detectable film erosion or property changes were noticed.
2. The thin-film gages, are relatively inexpensive when compared with piezoelectric gages.
3. Thin-film gages, with the appropriate circuit (hereafter the proper circuit will be implied), have a sensitivity to temperature of approximately $500 \mu\text{v}/\text{F}$. This is approximately 1 order of magnitude larger than the sensitivity of thermocouples, which is approximately $30 \mu\text{v}/\text{F}$.
4. Thin-film gages are exceptionally effective as pulse-signal generators for:
 - (a) Applications involving sudden temperature changes, as with shock waves.
 - (b) Applications requiring a very fast instrument response, i.e. a few microseconds.
5. Compared to piezoelectric gages the thin-film gages appear to be insensitive to vibration and mechanical shock. They are, however, good antennas and would probably not be suitable for use near large pieces of unshielded electrical equipment.
6. Thin-film gages will indirectly detect the relative

growth of the boundary layer and the subsequent transition from laminar flow to turbulent flow. With the equipment specifically set up for this purpose, one should be able to record the transition behavior with much more detail than that shown in Fig. 10b.

7. Thin-film gages will produce heat transfer data that is consistently higher than that predicted by Eq. 16, between $M_s = 1$ and $M_s = 2.5$. The difference appears to increase with shock Mach number, ranging from agreement near $M_s = 1$ to approximately 50 percent higher at $M_s = 2.5$ (Fig. 11). According to theory, however, the curve should have an inflection point around $M_s = 4$ (Ref. 32:118). Friedman and Fay (Ref:10), using an entirely different measuring system, and Argon and Xenon, also recorded much higher experimental heat transfer rates than was predicted by their respective theoretical equations. It is concluded that thin-film gages, as calibrated and used in this study, will detect heat transfer rates within the accuracy limits described in Appendix D.

8. Thin-film gages will indicate surface temperature histories for flow over a surface, that agree very well with theoretically predicted histories. The experimental data of this study also agrees well with experimental data from other sources (Ref. 14:29 and 32:117).

VII. Recommendations

Apparatus Improvements

The present heat transfer circuit picks up approximately 0.1 mv of stray electrical noise. By fabricating individual shielded circuits and locating the circuits virtually on top of the gages in small metal boxes, a large reduction in the reception of stray electrical noise should be achieved. This would allow amplification of the circuit output signal, without causing a corresponding increase in width of the oscilloscope trace. As is pointed out in Appendix D, reading the oscilloscope trace is one of the main sources for error associated with the present system. With this modification, the error magnitude associated with reading ΔE values from the oscilloscope trace should be reduced by a factor equal to the amplification factor.

Applications

The thin-film gage has numerous potential applications. It can be used as a device to determine surface temperature histories and heat transfer rates, or more simply as a pulse-signal generator in a velocity detection circuit. The thin-film heat transfer gage is especially applicable for use in shock tubes and tunnels. An application of the gages that has recently received attention, involves the study of thermal conductivity in the extreme high temperature gas behind a reflected shock wave. In fact, one of the most recent references found involving the use of thin-film gages was in this area (Ref. 6).

Bibliography

1. Bogdan, Leonard. High Temperature, Thin-Film Resistance Thermometers For Heat Transfer Measurement. NASA CR-26 Buffalo, New York: Cornell Aeronautical Laboratory, Inc., 1964.
2. Bowman, Robert M. Output of a Resistance Film Gage in Shock Tube Applications. Unpublished. Wright-Patterson AFB, Ohio: Air Force Institute of Technology, 1964.
3. Bradly, John N. Shock Waves in Chemistry and Physics. New York: John Wiley & Sons Inc., 1962.
4. Chabai, Albert J., and R. J. Emrich. "Measurement of Wall Temperature and Heat Flow in the Shock Tube," Journal of Applied Physics, 26:779-780 (1955).
5. Chen, Che Jen, and Raymond J. Emrich. "Investigation of the Shock-Tube Boundary Layer by a Tracer Method," The Physics of Fluids, 6, No. 1:1-9 (Jan. 1963).
6. Collins, D. J., R. Greif, and A. E. Bryson, Jr. "Measurement of the Thermal Conductivity of Helium in the Temperature Range 1600-6700°K," International Journal of Heat and Mass Transfer, 8:1209-1216 (Mar. 1965).
7. Eckert, E. R. G., and R. M. Drake, Jr. Heat and Mass Transfer. New York: McGraw-Hill Book Company, Inc., 1959.
8. Egan, Douglas S., and Robert A. Foster. Gas Dynamics Research with the Air Force Institute of Technology Shock Tube. AFIT Thesis. Wright-Patterson AFB, Ohio: Air Force Institute of Technology, 1956.
9. Fabian, G. J. Hypersonic Research Summary. CAL Rpt. No. AD-1118-A-11. Buffalo, New York: Cornell Aeronautical Laboratory, Inc., 1960. AD 233 152.
10. Friedman, Harvey S., and James A. Fay. "Heat Transfer from Argon and Xenon to the End Wall of a Shock Tube," The Physics of Fluids, 8, No. 11:1968-1975 (Dec. 1965).
11. Glass, I. I. Shock Tubes, Part I: Theory and Performance of Simple Shock Tubes. Utia Review No. 12 Toronto Canada: Institute of Aerophysics, University of Toronto, 1959.
12. Hall, Gordon J. Shock Tubes, Part II: Production of Strong Shock Waves; Shock Tube Applications, Design and Instrumentation. Utia Review No. 12. Toronto, Canada: Institute of Aerophysics, University of Toronto, 1958.

13. Hartunian, R. A., and R. L. Varwig. "On Thin-Film Heat-Transfer Measurements in Shock Tubes and Shock Tunnels." The Physics of Fluids, 5, No. 2:169-174 (Feb. 1962).
14. Hartunian, R., A. Russo, and P. Marrone. Boundary Layer Transition and Heat Transfer in Shock Tubes. CAL Rpt. #AD-118-A3. Buffalo, New York: Cornell Aeronautical Laboratory, Inc., 1959. AD 210 223.
15. Hertzberg, A. "The Application of the Shock Tube to the Study of the Problems of Hypersonic Flight," Jet Propulsion, 26, No. 7:549-568 (June 1956).
16. Konopka, Wayne. Heat Transfer Instrumentation for the Grumman Hypersonic Shock Tunnel. Grumman RM-287. Bethpage, New York: Grumman Research Dept., 1965. AD 234 728.
17. Lauver, M. R. "Shock Tube Thermal Conductivity," The Physics of Fluids, 7:611-612 (1965).
18. Marrone, P. V., and R. A. Hartunian. "Thin-Film Thermometer Measurements in Partially Ionized Shock Tube Flows," The Physics of Fluids, 2, 6:719-721 (Nov. (1959)).
19. Nagamatsa, H. T. "Shock Tube Technology and Design," Fundamental Data Obtained From Shock Tube Experiments, Edited by A. Ferri:86-183. New York: Pergamamon Press, 1961.
20. Rabinowicz, J., M. E. Jessey, and C. A. Bartsch. Resistance Thermometer for Heat Transfer Measurements in a Shock Tube. GALCIT Memorandum #33. Pasadena, California; California Institute of Technology, 1956.
21. Rott, N., and R. Hartunian. On Heat Transfer to the Walls of a Shock Tube. CAL Rpt. No. OSR-TN-55-422. Ithaca, New York: Cornell Aeronautical Laboratory Inc., 1955.
22. Scagnetti, Monique, and Jean Crabol. "East-Response, Platinum-Film Temperature Probes," La Recherche Ae'rospatials, 97:23-30 (Nov. 1963).
23. Seginer, A., A. Cohen, and J. Rom. "Calibration of Thin Film Resistance Thermometers for Heat Flux Measurements in the Shock Tube," Israel Journal of Technology, 3, No. 1:25-30 (Feb. 1965).
24. Skinner, G. T. "Calibration of Thin-Film Backing Materials," ARS Journal, 31, No. 5 (May 1961).

25. Skinner, G. T. A New Method of Calibrating Thin Film Gage Backing Materials. CAL Rpt. No. 105. Buffalo, New York: Cornell Aeronautical Laboratory, Inc., 1962. AD 282 409.
26. Sturtevant, Bradford, and Erik Slachmuylders. "End-Wall Heat-Transfer Effects on the Trajectory of a Reflected Shock Wave," The Physics of Fluids, 7, No. 8: 1201-1207 (Aug. 1964).
27. Taylor, B. W. Development of a Thin Film Heat-Transfer Gage For Shock Tube Flows. Utia TN No. 27. Toronto, Canada: Institute of Aerophysics, University of Toronto, 1959. AD 230 721.
28. Truitt, R. W. Fundamentals of Aerodynamic Heating. New York: The Ronald Press Co., 1960.
29. Van Driest, E. R. Investigation of Laminar Boundary Layer in Compressible Fluids Using the Crocco Method. NACA TN 2597. Washington, D C: National Advisory Committee for Aeronautics, 1952.
30. Vidal, R. J. Model Instrumentation Techniques for Heat Transfer and Force Measurements in a Hypersonic Shock Tunnel. WADC TN 56-315. Buffalo, New York: Cornell Aeronautical Laboratory, Inc., 1956. AD 972 38.
31. Vidal, R. J., and J. H. Hilton. The Construction and Application of a Rapid Response Resistance Thermometer Probe. CAL Rpt. IM-1062-A-1. Buffalo, New York: Cornell Aeronautical Laboratory, Inc., 1956.
32. Weatherston, R. C., A. L. Russo, W. E. Smith, and P. V. Marrone. Gasdynamics of a Wave Superheater Facility for Hypersonic Research and Development. AFOSR TN 59-107. Buffalo, New York: Cornell Aeronautical Laboratory, Inc., 1959. 210 223.
33. Weisblatt, Herbert, and A. Clemente. Development of a 0.005-inch Wide Gold Thin Film Resistance Thermometer Heat Transfer Gage For Use in Shock Tubes. AVCO Tech. Memorandum. Wilmington, Mass: Research and Advanced Development Division AVCO Corporation, 1960. 243 225.
34. Wittliff, Charles E., and George Rudinger. Summary of Instrumentation Development and Aerodynamic Research in a Hypersonic Shock Tunnel. WADC TR 58-401. Buffalo, New York: Cornell Aeronautical Laboratory, Inc., 1958. AD 155 758.

Appendix A

Gage Construction

The purpose of this appendix is to provide a detailed description of the procedure used to construct the thin-film gages used in this study. The process described herein reflects the influence of references and the influence of personal correspondence and discussions with others who have fabricated and used these gages. Over 100 gages were made before sufficient experience was accumulated to permit rapid, reliable gage construction. The gages were always made in sets of five or more, and required approximately two days per finished set (including oven time). There are four main steps in this process:

- 1) Procuring and preparing the materials
- 2) Applying the film to the backing material
- 3) Firing the film onto the backing material
- 4) Attaching the electrical leads to the film

Procuring and Preparing the Materials

Several special items and pieces of equipment were used in this process:

- 1) An oven capable of sustaining temperatures of 700F with the door opened slightly to provide ventilation, and 1300F with the door closed. The oven should have a volume capacity sufficient to accommodate at least a dozen prospective gage blanks, so that several gages may be made at one time.

- 2) A quantity of Liquid Bright Platinum #05-X, (Hanovia Chemical and Manufacturing Company of East Newark, New Jersey). One fluid ounce is enough for approximately 1000 gage films 1/2 in. long and 1/16 in. wide.
- 3) A set (body and hardener) of E-Solder #3021, Silver Epoxy (Epoxy Products Inc., Irvington, New Jersey). One set of 1 oz tubes is enough for approximately 100 gages.
- 4) A quantity of quartz gage blanks. These blanks will act as backing material for the platinum film and are cut, drilled, and polished to their final dimensions prior to having the film applied. The holes in the blanks were drilled using a Cavitron (ultrasonic vibration drill). To prevent the drill from breaking out on the back surface of the blank, the blanks were fastened to a sheet of soda glass with high temperature wax prior to drilling. Once the blanks were completely formed, they were thoroughly washed in commercial acetone, and then "burned" (just short of melting) with an oxygen rich torch to remove all surface residues. The blanks were then handled with tweezers until after the film was applied. The quartz blanks are illustrated in Fig. 3 and Appendix G.

Applying the Film to the Backing Material

The desired resistance of the gages was approximately

GAM/ME/66A-3

50 ohms. The gage resistance is controlled by the length and cross-sectional area (perpendicular to the direction of current flow) of the film. Since the length is fixed by the geometry of the gage blank, the gage width and thickness must be controlled. Also, regardless of the dimensions, the film must be as uniform as possible. Several methods of film application were attempted, but the simplest, quickest, and most easily duplicated method was to draw the film on the gage blank using an old-fashioned dip point (size 1) pen. The natural line formed by the pen was found to yield a uniform film with approximately the desired resistance.

The pen was dipped in the liquid platinum and all possible liquid was rubbed off on the bottle lip. The film was then drawn, with the aid of a straight edge, across the gage blank beginning and terminating at the lead attachment holes. A generous coat of the liquid platinum was then applied around (inside and outside) the lead attachment holes.

Firing the Film onto the Backing Material

The freshly painted gages were then placed in the unheated oven and raised in temperature to 700F with the door open approximately 1/2 in. to provide ventilation (the rate of change of temperature was roughly 10F/min). After the oven had stabilized at 700F, the oven door was closed and the temperature was raised to 1300F for 4 to 5 hours. The closed oven was then allowed to cool slowly to room temperature. This procedure was 100 percent successful in achieving a good bond between the film and the quartz.

Attaching the Electrical Leads to the Film

Several methods were successfully used to attach leads to the gage film. Although the most popular method in the literature consisted of baking a layer of Liquid Silver (Hanovia #467) over the ends of the platinum film and then soldering lead wires directly to the cured silver using low temperature solder (Tektronix #251-0514-00 solder). However, the slightest overheating during the soldering operation would oxidize the silver and ruin the gage. For use in applications involving gage temperatures up to 300F the epoxy method seemed to be definitely superior for the following reasons:

- 1) The epoxy firmly anchored the lead wires in the holes independent of any electrical consideration.
- 2) The cured epoxy demonstrated a stable, but negligible resistance.
- 3) The application of epoxy did not involve any critical steps, and mistakes could be washed off with acetone (prior to curing).

Lead wires were then prepared as for conventional soldering. Solid copper wire was found to make better lead material than stranded wire, because the solid wire was easier to prepare and handle. The two parts of the epoxy were mixed on a glass dish as directed by the instructions. The dressed end of each wire was individually dipped into the epoxy; then, using the wires as applicators, both holes in the quartz were generously coated with epoxy. A sufficient amount of epoxy was used to form a "bead" on the thin film

side of the hole, thus insuring a good contact with the platinum film (Fig. 6). Due to difficulty in handling the gages in the soft epoxy condition, the epoxy was allowed to room harden until firm (approximately two hours depending on the room temperature). After the epoxy had solidified the gages were placed in the oven and the temperature was raised to approximately 200F for 3 or 4 hours. This second baking promoted the hardening of the epoxy and acted as a stress reliever for the thin film. The closed oven was then allowed to cool to room temperature before removing the gages. If desired, the epoxy "beads" were removed by pressing a piece of masking tape over the finished gage, and then filing the "beads" down flush with the tape. The tape protected the thin film and at the same time assured a thin, but finite epoxy coating.

Appendix BGage Calibration

Calibration data for the thin-film gages were obtained by pulsing a known, and essentially constant, electrical charge through the gages, and recording on film the ΔE vs t displayed on an oscilloscope.

The gage calibration circuit is shown in Fig. 7. With the bridge minutely (but intentionally) out of balance (± 0.0002 volts), and a fixed resistor in place of the gage, the steady-state oscilloscope response to the circuit was photographed. Then, without disturbing the circuit, the mercury switch was turned off and the capacitor was allowed to charge. The mercury switch was then closed and the resulting oscilloscope response was recorded on the same photograph with the steady state response. A typical result of this action is shown in Fig. B-1. As can be seen, the discharge voltage is well described by a step function for the first 1000 μsec .

Replacing the fixed resistor with a thin-film gage and duplicating the above procedure, the circuit response was again recorded (Fig. B-2). An analysis of Fig. B-2 reveals that the $\Delta E(t)$ trace is well described by a parabolic equation for the first 1000 μsec . The surface temperature solution of the classical one-dimensional heat conduction equation was shown to be a parabolic function of time for a constant heat transfer rate (Eq. 4), and the film temperature (which is almost literally the surface temperature) was shown to be directly related to ΔE (Eq. 10).

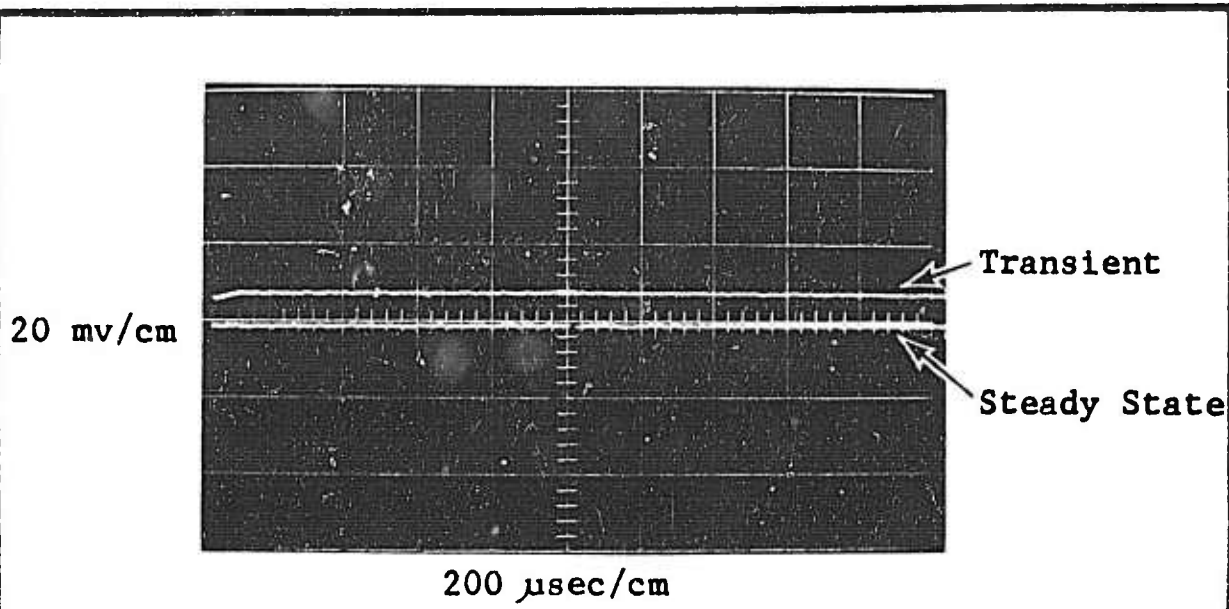


Figure B-1

A Typical Calibration Response Using a
Fixed Carbon Resistor in Place of the Gage

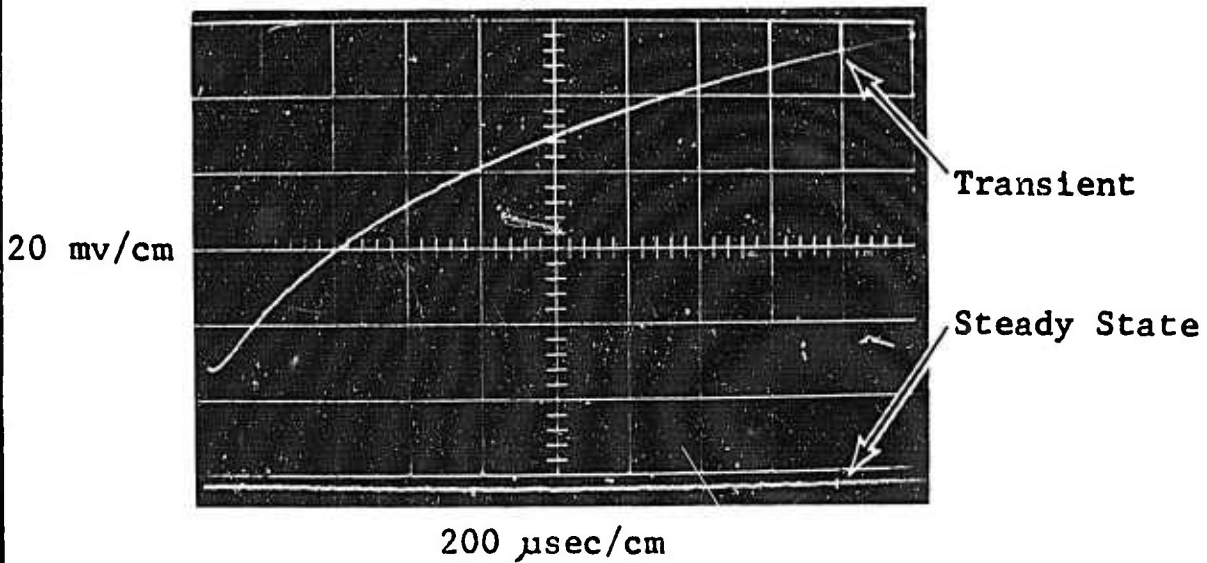


Figure B-2

A Typical Calibration Response Using
A Thin-Film Gage

With the ammeter in the circuit, a slight hook was recorded in the calibration trace near $t = 0$ (Fig. B-2). With the ammeter switched out of the circuit this hook could not be recorded. The hook in the trace was therefore attributed to the inductive property of the meter. In any case the quantity $\Delta E/t^{1/2}$ is essentially a constant for values of t between 100 and 1000 μsec . This would, according to theory, indicate a constant heat transfer rate. The equation relating ΔE of the bridge circuit to a constant rate of heat transfer through the gage was shown to be (Eq. 12).

$$q = \frac{(\pi k \rho c)^{1/2}}{2\alpha} \left[\frac{R_0 + R_2}{R_2 I_0 R_0} \right] \frac{\Delta E}{t^{1/2}} \quad (\text{B-1})$$

The heat transfer rate to the gage is given by

$$q = \frac{I^2 R_0}{\text{Area}} \quad (\text{B-2})$$

For q to be a true step function the thin-film must be uniform in thickness and in width, and $\Delta R/R_0$ must be small. The thickness and width are controlled during gage construction, and $\Delta R/R_0$ is controlled by the voltage on the capacitor. For this study $\Delta R/R_0$ maximum was approximately 0.5 percent of R_0 . The current through the gage at any time is given by

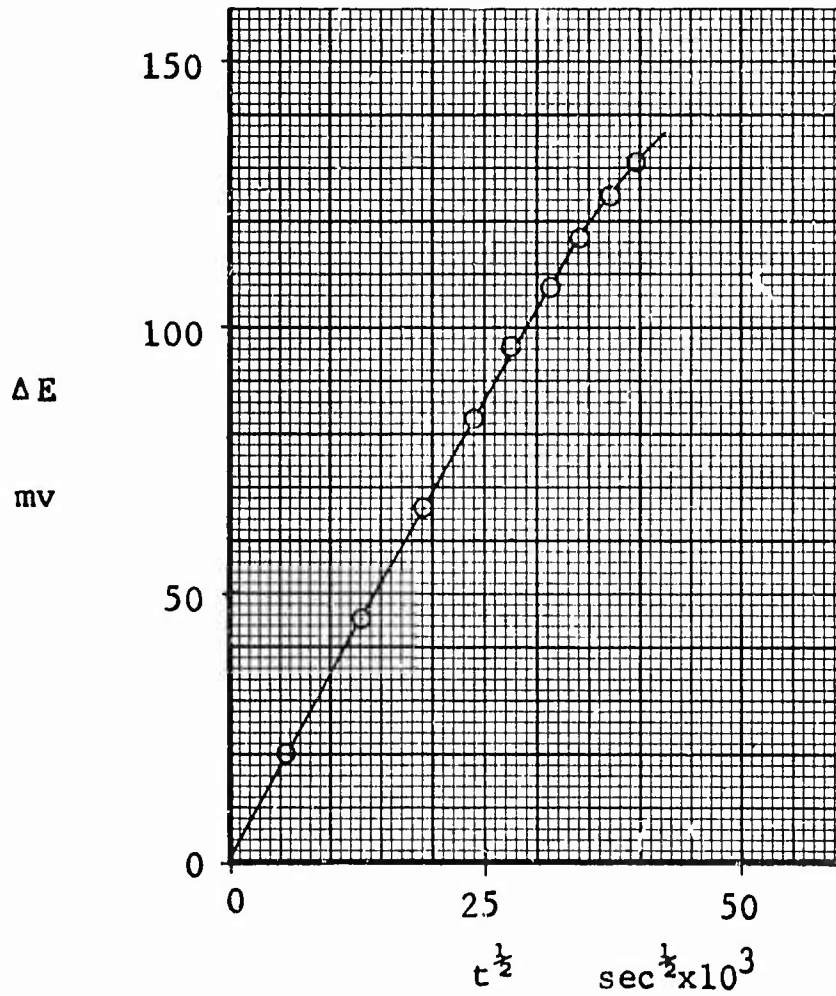
$$I_0 = \frac{V_b}{R_0 + R_2} \quad (\text{B-3})$$

As can be seen from the calibration circuit (Fig. 7) and from the calibration response using a fixed resistor (Fig. B-1), V_b exactly equals the source voltage the instant the Hg. switch is closed and is essentially constant for the first 1000 μ sec.

An equation relating known or measureable quantities to the bulk heat transfer parameter of the gage was obtained by combining Eqs. (B-1), (B-2) and (B-3):

$$\beta = \frac{(\pi k \rho c)^{\frac{1}{2}}}{2\alpha} = \frac{R_2 R_o^2 V_b^3}{A(R_o + R_2)^4} \frac{t^{\frac{1}{2}}}{\Delta E} \quad (B-4)$$

The value of $\Delta E/t^{\frac{1}{2}}$ is constant for a constant rate of heat transfer and is illustrated for a typical gage in Fig. B-3. As time increases the curve begins to deviate significantly from a straight line, as expected, due to the decay in the pulse voltage from the capacitor. Notice that the absolute magnitude of ΔE is not required. For this reason no effort was made to balance the bridge closer than ± 0.0002 v.



(Data from gage III-4 calibration photograph 21Dec65-1)

Figure B-3

Converted Calibration Curve

(ΔE vs. t to ΔE vs. $t^{1/2}$)

Appendix CSample CalculationsTypical Calibration Data

As was described in Appendix B, the calibration oscilloscope trace (ΔE vs. t) was converted to a straight line by replotting coordinates ΔE and $t^{\frac{1}{2}}$. The slope of this line and other recorded data, for the calibration of gage III-4, 21 Dec. 1965 was

$$\Delta E/t^{\frac{1}{2}} = 3.43 \text{ (From Fig. B-3)}$$

$$V_o = 23.59 \text{ volts (across the capacitor, Fig. 7)}$$

$$R_{2 \text{ cal}} = 51.617 \text{ ohms}$$

$$R_{o4} = 49.73 \text{ ohms}$$

$$A = 66.3 \times 10^{-6} \text{ ft}^2$$

$$\text{Conversion factor: } 1000 \text{ watts} = 0.9478 \text{ B/sec}$$

Calculation of the Gage Coefficient β

The value of the bulk heat transfer parameter for the gage was computed using Eq. B-4:

$$\beta = \frac{(\pi k \rho c)^{\frac{1}{2}}}{2\alpha} = \frac{R_2 R_o^2 V_o^3}{A(R_o + R_2)^4} \frac{t^{\frac{1}{2}}}{\Delta E} \quad (\text{C-1})$$

$$\beta = \frac{(51.617)(49.73)^2(23.59)^3(.948)(10^3)}{(66.25)(10^{-6})(101.347)^4(3.43)}$$

$$\beta = 66.3 \text{ B/ft}^2 \text{ sec}^{\frac{1}{2}}$$

Typical Run Data

The following data was recorded for run 20, 22 Dec. 1965; using gage III-4 mounted flush in the shock tube side wall.

$$\Delta E = 0.2339 \times 10^{-3} \text{ volts (from photograph)}$$

$$R_{2_{op}} = 928.418 \text{ ohms}$$

$$I_o = 10 \text{ ma}$$

$$R_o = 0.001065 \text{ ohms/ohm F}$$

$$1/V_s = 456 \text{ } \mu\text{sec/ft (from timer)}$$

$$T_1 = 82 \text{ F}$$

$$P_1 = 0.84 \text{ in. Hg}$$

$$P_a = 29.28 \text{ in. Hg}$$

$$P_4/P_1 = 34.9$$

$$P_2/P_1 = 4.18 \text{ (from Ref. 11:Fig. 2.2.10a)}$$

Note: Sufficient variation was noted in the photographs to require the following conversion procedure for each photograph:

$$\Delta E = \frac{\text{(Trace step measurement)}}{\text{(The local 1 cm grid measurement)}} \text{ (vertical grid scale)}$$

Calculation of the Shock Mach Number

The shock mach number was computed using V_s and T_1 (converted to V_a):

$$M_s = \frac{V_a}{V_s} = \frac{877}{456} = 1.925 \quad (C-2)$$

Calculation of the Pressure Behind the Shock Wave

The pressure behind the moving shock wave was computed in the following manner:

$$P_2 = \frac{P_2}{P_1} \frac{P_1}{P_a} \frac{P_a}{P_o} P_o \quad (C-3)$$

$$P_2 = (4.18)(.0287)(.980)(1 \text{ atm})$$

$$P_2 = 0.1175 \text{ atm}$$

$$P_2^{\frac{1}{2}} = 0.343 \text{ atm}^{\frac{1}{2}}$$

Calculation of the Wall Surface Temperature Change

The magnitude of the step in ΔE immediately after shock wave passage was obtained directly from the recorded oscilloscope trace. This value for ΔE was then reduced to ΔT using Eq. 10:

$$\Delta T = \frac{R_o + R_2}{\alpha R_2 R_o I_o} \Delta E \quad (C-4)$$

$$\Delta T = \frac{(978.168) \Delta E}{(.001065)(928.42)(49.75)(10 \times 10^{-3})}$$

$$\Delta T = 1985 \Delta E$$

$$\Delta T = 0.4635 F$$

This ΔT represents the step in wall surface temperature for the laminar boundary layer flow condition immediately after passage of the shock wave. To simplify data presentation, ΔT was divided by $P_2^{\frac{1}{2}}$:

$$\frac{\Delta T}{P_2^{\frac{1}{2}}} = \frac{0.4635}{6.343} = 1.35 F/\text{atm}^{\frac{1}{2}} \quad (\text{C-5})$$

Calculation of the Heat Transfer Rate

If the rate of heat transfer is not a constant, it may be computed from measured data using Eqs. 6 or 13. Both of these equations are difficult to evaluate manually when ΔT (or ΔE) is not constant. (A manual integration method for computing q , using a nearly identical equation, is given by Taylor) (Ref. 27:17). However, when ΔT is constant the computation of the heat transfer rate is much less complicated. A typical example of the calculation for a variable q and a constant ΔT would be (Eq. 13)

$$q = \beta \frac{R_0 - R_2}{I_0 R_2 R_0} \left[\frac{\Delta E(t)}{(t)^{\frac{1}{2}}} - (0) \right] \quad (\text{C-6})$$

$$q = 66.3 \frac{(978.168) \Delta E}{(928.42)(49.75)(10 \times 10^{-3})t^{\frac{1}{2}}}$$

$$q = 140.3 \frac{\Delta E}{t^{\frac{1}{2}}} \text{ B/ft}^2 \text{ sec}$$

$$q = \frac{0.0328}{t^{\frac{1}{2}}} \text{ B/ft}^2 \text{ sec}$$

For purposes of comparison and plotting, the heat transfer rate was multiplied by $t^{\frac{1}{2}}$ and divided by $P_2^{\frac{1}{2}}$:

$$q \frac{t^{\frac{1}{2}}}{P_2^{\frac{1}{2}}} = \frac{0.0328}{0.343} \quad (\text{C-7})$$

$$q \frac{t^{\frac{1}{2}}}{P_2^{\frac{1}{2}}} = 0.0957 \text{ B/ft}^2 \text{ sec}^{\frac{1}{2}} \text{ atm}^{\frac{1}{2}}$$

Appendix D
Accuracy Analysis

The Accuracy of Recorded Values

Table D-1 lists the various variables that were recorded, the tolerance of the recording instruments, and the assumed variation involved with reading the instruments. Table D also gives representative values for the variables, and a computed quantity which represents the (possible) combined deviation from the reference value.

Accuracy of Computations

All calculations in this study were made using a conventional slide rule. Because any such estimate would be highly subjective, no attempt was made to estimate the error potential from this source.

Gage Calibration

Gage calibration involves three potential sources of error. Errors arising from theoretical assumptions, errors stemming from variations in data recording, and errors introduced by computations. The limitations and assumptions involved with the theoretical analysis are discussed in Appendix B. The errors introduced in this realm are assumed to be at least an order of magnitude smaller than those associated with data recording and will be neglected.

The essence of gage calibration is the determination of the bulk heat transfer parameter β . It would, therefore, be meaningful to investigate the potential error in β due to cumulative deviation in the data.

Table D-1

Data Error Analysis

Recorded Variable	Instrument Tolerance	Reading Variation (estimate)	Typical Values	Combined Deviation (magnitude)	Combined Deviation (percent)
Resistance (ohms)	±0.001	exact	2 50 1000	0.0001 0.0001 0.0001	6.15 0.002 0.0001
Steady State Voltage (v)	±0.02%	±0.05	24	0.0553	0.23
Voltage Change (trace) (mv)	±0.02%	±0.05	0.5 500	0.0525 15	10.05 0.03
Time (trace) (µsec)	±0.02%	±4	100 80,000	4.02 22	4.02 0.0275
Shock Wave Transit Time (µsec)	±1	exact	500	1.0	0.20
Shock Wave Transit Distance (in.)	exact	±0.1	12	0.1	0.83
Steady State Current (ma)	±5.0%	±0.1	10	0.6	6.00
Film Area (in. ²)	±1.0%	±10.0%	0.009 (.03x.3)	0.0012	12.22
Temperature (F)	±2.0	±0.2	82	2.20	2.68
Temperature Change (gage calibration)	negligible	±0.2	50	0.20	0.40

$$\beta = \frac{R_2 R_0^2 V_0^3 t^{\frac{1}{2}}}{A(R_0 + R_2)^4 \Delta E} \quad (D-1)$$

taking values from Table D-1:

$$\beta = \frac{(50)(50)^2(24)^3(80,000)^{\frac{1}{2}}}{(.009)(100)^4(500)} = 1088 \frac{\text{watt sec}^{\frac{1}{2}}}{\text{in.}^2} \quad (D-2)$$

The maximum deviation of β occurs when the numerator is maximum and the denominator is minimum:

$$\beta_{\max} = \frac{(R_2 + \Delta R)(R_0 + \Delta R_0)^2(V_0 + \Delta V_0)^3(t + \Delta t)^{\frac{1}{2}}}{(A - \Delta A)(R_0 + R_2 - \Delta R_0 - \Delta R_2)^4(\Delta E - \Delta \Delta E)} \quad (D-3)$$

$$\beta_{\max} = \frac{(50.001)(50.001)^2(24.0553)^3(80,022)^{\frac{1}{2}}}{(.0078)(99.998)^4(485)} = 1300 \frac{\text{watt sec}^{\frac{1}{2}}}{\text{in.}^2} \quad (D-4)$$

Converting to a percentage basis, and calling the result the β deviation limit:

$$\beta_{\text{dev lim}} = \frac{\beta_{\max} - \beta}{\beta}(100) = 19.5\% \quad (D-5)$$

It is most unlikely that this cumulative error would be achieved in practice, but the computation does reveal the relative influence of the variables. By comparing Eq. D-2 and D-4 it can be seen that ΔE and A contribute the bulk of this potential error, and that terms raised to powers have relatively little effect, which was unexpected. Obviously the

area and voltage change should be measured and recorded as accurately as possible. In actual practice, β is believed to be accurate to approximately 5 percent. This opinion is supported by comparing the results shown in Table 1 with numerous other sources.

The value for α was computed directly from the definition:

$$\alpha = \frac{\Delta R}{\Delta T R_0} \quad (D-6)$$

$$\alpha = \frac{(2)}{(50)(50)} = 0.000802 \frac{\text{ohms}}{\text{ohm F}}$$

$$\alpha_{\max} = \frac{\Delta R + \Delta\Delta R}{(\Delta T - \Delta\Delta T)(R_0 - \Delta R_0)} \quad (D-7)$$

$$\alpha_{\max} = \frac{2.001}{(49.8)(49.999)} = 0.0008075 \frac{\text{ohms}}{\text{ohm F}}$$

Converting to a percentage basis and calling the result the α deviation limit:

$$\alpha_{\text{dev lim}} = \frac{\alpha_{\max} - \alpha}{\alpha} 100 = 0.686\% \quad (D-8)$$

Temperature Change Measurements

Only the recording of the experimental data will be investigated here. The assumptions involved in the

theoretical analysis, and the degree to which they were achieved, is covered in Section II.

$$\Delta T = \frac{R_o + R_2}{\alpha R_o R_2 I_o} \Delta E \quad (D-9)$$

Using values from Table D-1 and the solution of Eq. D-6:

$$\Delta T = \frac{1050}{(.0008075)(50)(1000)(10)} (.5) = 1.30 \text{ F} \quad (D-10)$$

The ΔT corresponding to the maximum deviation was computed using

$$\Delta T_{\max} = \frac{(R_o + \Delta R_o + R_2 + \Delta R_2)(\Delta E - \Delta \Delta E)}{(\alpha - \Delta \alpha)(R_o - \Delta R_o)(R_2 - \Delta R_2)(I_o - \Delta I_o)} \quad (D-11)$$

Using values from Table D-1 and Eq. D-7:

$$\Delta T_{\max} = \frac{(1050.002)(.5525)}{(.0007965)(49.998)(999.998)(9.4)} \quad (D-12)$$

$$\Delta T_{\max} = 1.55 \text{ F}$$

$$\text{Therefore: } \Delta T_{\text{dev lim}} = \frac{\Delta T_{\max} - \Delta T}{\Delta T} (100) = 19.24\% \quad (D-13)$$

The computation reveals that the values for ΔE and I_0 should be measured and recorded as accurately as possible, as they clearly contribute the bulk of the potential error. At first glance, one might inquire as to why E/R was not used in lieu of I , since it apparently can be measured and recorded with much greater accuracy. This apparent alternative could not be used because the voltage across the operating circuit bridge (Fig. 2) was unknown. A variable resistor, which is located between the bridge and the voltage source causes the bridge voltage to be a variable. The deviation limit of 19.24 percent is not likely to be achieved. A conservative, but realistic, estimate for the accuracy limits of ΔT using the apparatus of this study is ± 10 percent.

Heat Transfer Measurements

The theoretical analysis, with the assumptions and the degree to which they were met, is covered in Section II. As above, only the recording of the experimental data will be covered here. The equation used to calculate the heat transfer rate was Eq. 13. However, it was simplified somewhat, since the integral had a value of zero for all the data reduced for this study.

$$q = \beta \frac{R_0 + R_2}{I_0 R_2 R_0} \frac{\Delta E}{t^{\frac{1}{2}}} \quad (D-14)$$

Equation D-14 was modified slightly to cause the plotted values to take a more desirable curve shape. This resulted in an equation of the form

$$\frac{q t^{\frac{1}{2}}}{P_{\text{atm}}^{\frac{1}{2}}} = \beta \frac{R_0 + R_2}{I_0 R_0 R_2} \frac{\Delta E}{P_{\text{atm}}^{\frac{1}{2}}} \quad (\text{D-15})$$

but,

$$\beta \frac{R_0 + R_2}{I_0 R_0 R_2} \Delta E = \beta \alpha \Delta T \quad (\text{D-16})$$

therefore:

$$\frac{q t^{\frac{1}{2}}}{P_{\text{atm}}^{\frac{1}{2}}} = \frac{\beta \alpha \Delta T}{P_{\text{atm}}^{\frac{1}{2}}} \quad (\text{D-17})$$

because $P_{\text{atm}}^{\frac{1}{2}}$ appears on both sides of the equation and is equal to itself, it will not be considered in the remaining discussion. Therefore, it remains only to determine the error associated with $\beta \alpha \Delta T$. Taking the results of Eqs. D-2, D-6, and D-10

$$\beta \alpha \Delta T = (1088)(.000802)(1.30) \quad (\text{D-18})$$

$$\beta \alpha \Delta T = 1.135 \frac{\text{watt sec}^{\frac{1}{2}} \text{ ohms}}{\text{in.}^2 \text{ ohm}}$$

The value corresponding to the maximum deviation of $\beta \alpha \Delta T$ was computed using

$$(\beta \alpha \Delta T)_{\text{max}} = (\beta_{\text{max}})(\alpha_{\text{max}})(\Delta T_{\text{max}}) \quad (\text{D-19})$$

Using values from Eqs. D-4, D-7, and D-12

$$(\beta\alpha\Delta T)_{\max} = (1300)(.0008075)(1.55)$$

$$(\beta\alpha\Delta T)_{\max} = 0.491 \frac{\text{watt sec}^{\frac{1}{2}} \text{ ohms}}{\text{in.}^2 \text{ ohm}}$$

$$\text{therefore: } (\beta\alpha\Delta T)_{\text{dev lim}} = \frac{0.491}{1.135} (100) = 43.3\% \quad (\text{D-20})$$

This error in actual practice would be totally unacceptable. Even as a potential error this value is excessive. What is believed to be a more realistic value is obtained if the apparent accuracy of β is used (approximately 5 percent), and a value of 10 percent is assumed for ΔT . These estimated values, along with α , yield a more realistic maximum error (rme).

$$(\beta\alpha\Delta T)_{\text{rme}} = \frac{(1.05)(1088)(110)(1.30)(.008075) - 1.135}{1.135} (100) \quad (\text{D-21})$$

$$(\beta\alpha\Delta T)_{\text{rme}} = \frac{0.184}{1.135} (100) = 16.22\%$$

To avoid achieving these large potential errors it is essential that care be exercised when taking and recording data. This is especially true when items being measured and recorded are: The current, oscilloscope trace values, and the area of the thin film.

Appendix E

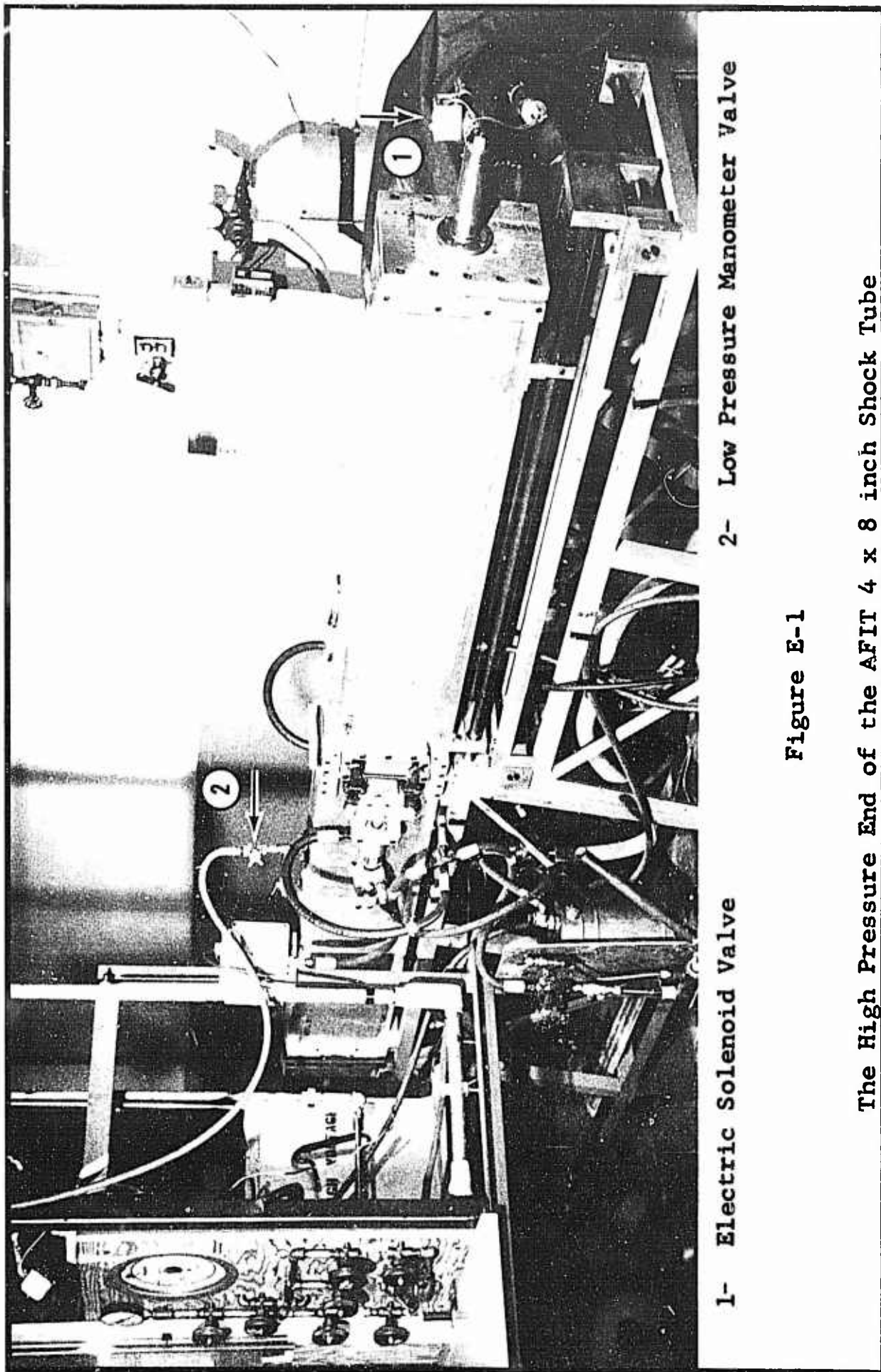
Shock Tube Modifications

Modifications of the Shock Tube Firing Mechanism

A large electrical noise which prematurely triggered the oscilloscope or counter apparatus was noted every time the shock tube was fired. The noise level was not precisely measured, but was at least 3 orders of magnitude greater than the pulse signals being used to trigger the electric timer (Fig. 5). Investigation revealed the electric solenoid valve in the diaphragm rupturing system (Fig. E-1) as the noise source. This electric valve controlled the air pressure which actuated the diaphragm rupture plunger. (For more details on the diaphragm rupture mechanism see Ref. 8: 14). The electric valve, and the pressure gage for the rupture system (which is hidden behind the shock tube in Fig. E-1), were both removed. The pressure gage was relocated, and the electric valve was replaced with a manually operated (but fast acting) valve and is shown along with the relocated gage in Fig. E-2.

Relocation of the Low Pressure Manometer Valve

The low pressure manometer valve (which must be closed prior to firing the shock tube to prevent violent fluctuations of the liquid mercury) is shown in Fig. E-1. This faucet type valve was replaced with an easily operated lever valve; and was relocated next to the mercury manometer (within easy reach of the shock tube operator), as shown in Fig. E-2.

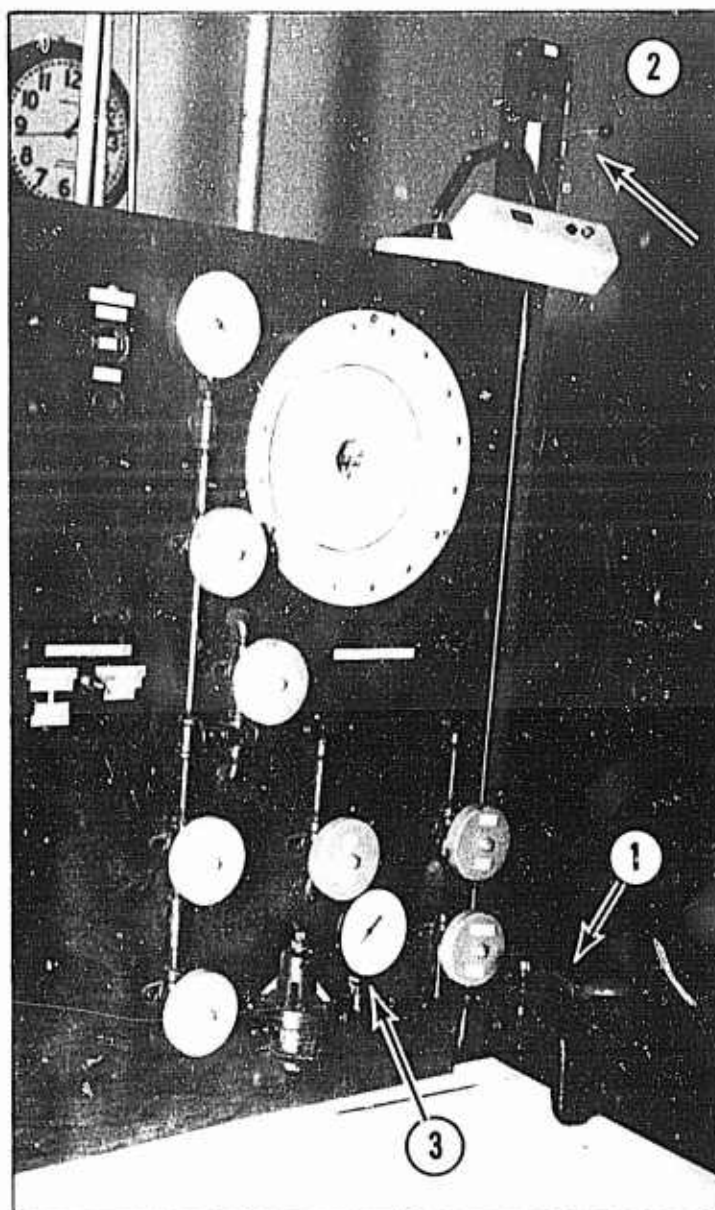


1- Electric Solenoid Valve

2- Low Pressure Manometer Valve

Figure E-1

The High Pressure End of the AFIT 4 x 8 inch Shock Tube



- 1- Manual Diaphragm Rupture Valve
- 2- Rupture Mechanism Pressure Gage
- 3- Low Pressure Manometer Valve

Figure E-2

The Modified Shock Tube Control
Console

Appendix F

Commercial Apparatus

Amplifier; Type 1121 Amplifier; Tektronix, Inc.;
Portland, Oregon.

Bridge; Resistance Bridge Catalogue No. 4725; Leeds
and Northrup Co.; Philadelphia, Pa.

Camera; Polaroid (with Fairchild Type F-296 Oscillo-
scope) Cambridge, Massachusetts.

Galvanometer; Catalogue No. 2430-C; Leeds and Northrup
Co.; Philadelphia, Pa.

Microscope; Traveling Microscope, No. 2776P; Gaertner
Scientific Corporation; Chicago, Ill.

Oscilloscope; Type 531; Tektronix, Inc.; Portland,
Oregon.

Oven; Type 1300 Furnace, Model #FA1315M; Thermolyne
Corporation; Dubuque, Iowa.

Preamplifier; Type 53/54 plug-in unit; Tektronix, Inc.;
Portland, Oregon.

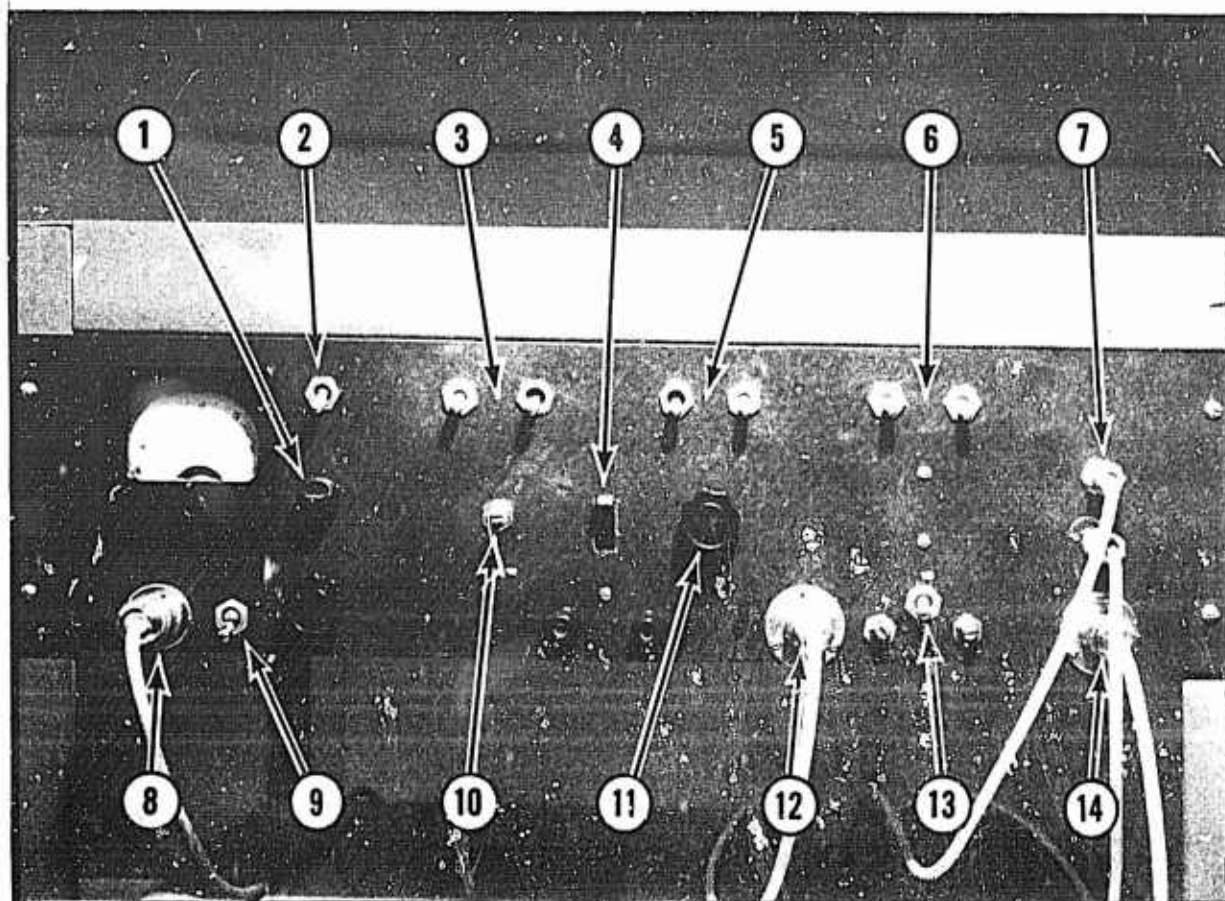
Thermocouple Bridge; No. 42738; Rubicon Co.;
Philadelphia, Pa.

Timer; Berkeley Time Interval Meter Model 5120;
Beckman Instruments, Inc.; Richmond, California.

GAM/ME/66A-3

Voltmeter; Model 901, Weston Electrical Instrument
Corporation; Benton Harbor, Mich.

Appendix G
Control Panel Layout
and
Drawings of the Gage Mounting Components

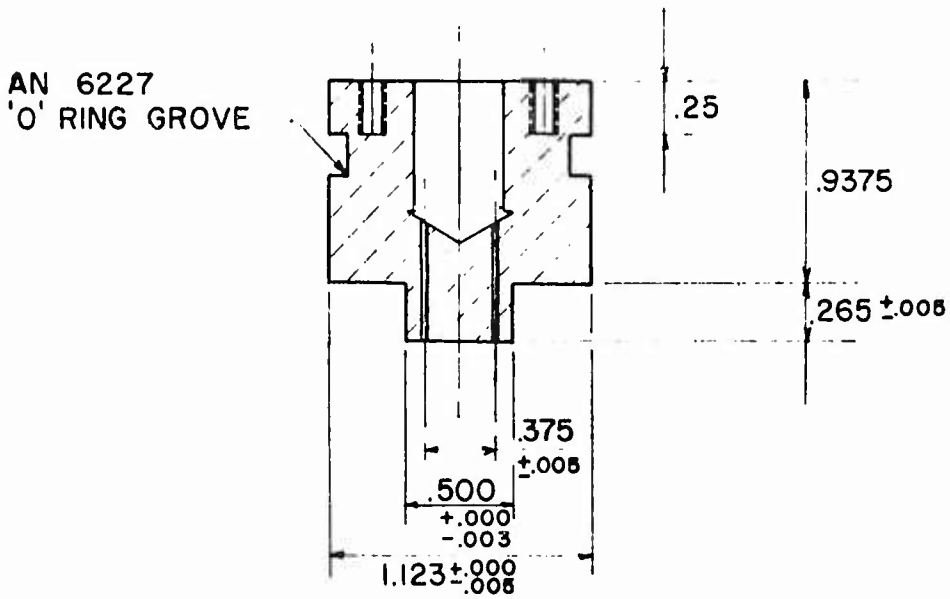
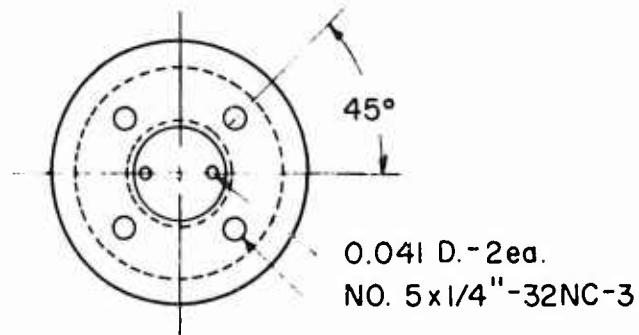


- 1- Current Set Knobs (2)
- 2- Ammeter Switch
- 3- Operate Circuit Switches (2)
- 4- Mercury Switch
- 5- Calibrate Circuit Switches (2)
- 6- Velocity Circuit Switches (2)
- 7- Gage Terminals, Common (2)
- 8- Battery
- 9- Power Switch
- 10- Operate Circuit Bridge Balance
- 11- Calibrate Circuit Bridge Balance
- 12- Oscilloscope, Calibrate Circuit
- 13- Velocity Circuit Amplifier Switch
- 14- Oscilloscope, Operate Circuit

Figure G-1

Heat Transfer Gage Control Panel

GAGE HOLDER
(Lucite)



GAGE BLANK
(Quartz)

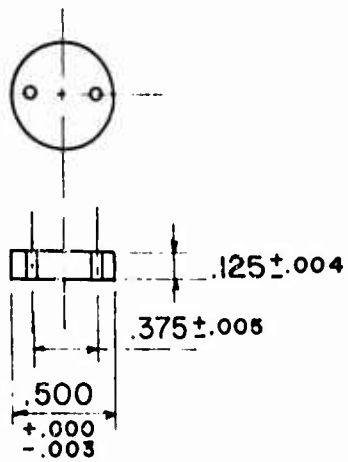
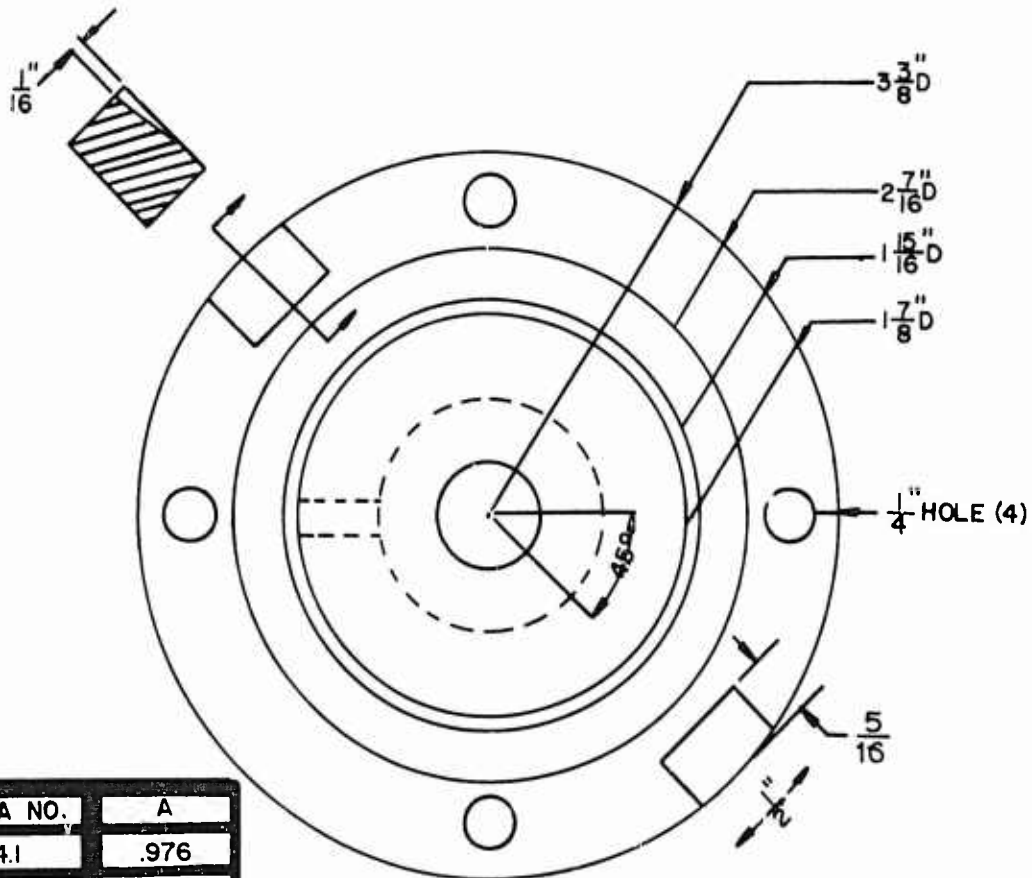
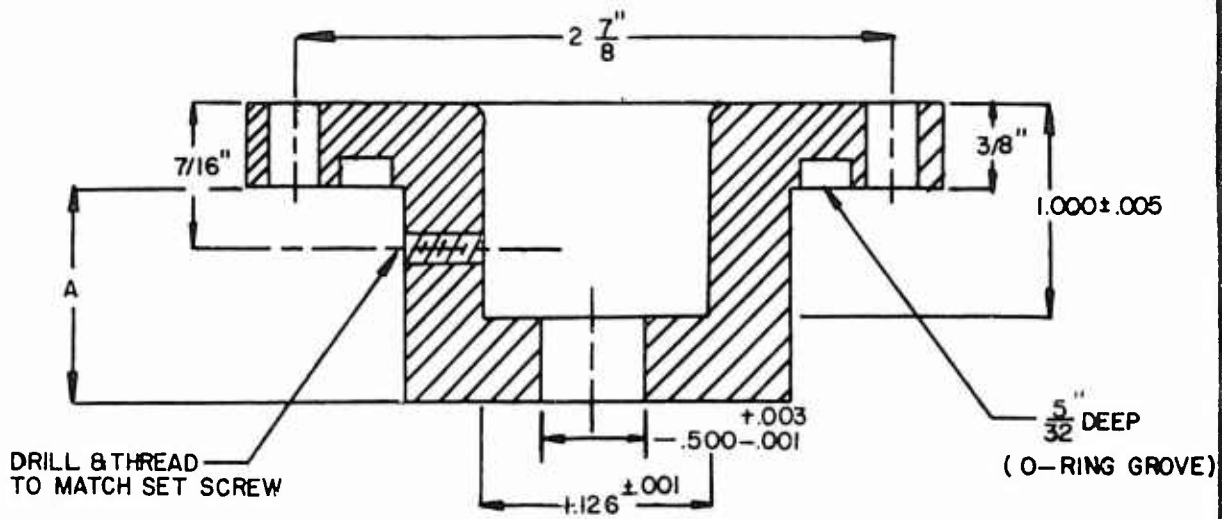


Figure G-2
Gage Holder and Gage Blank



STA NO.	A
4.1	.976
4.2	.974
4.3	.974
5.1	1.000
5.2	1.000

Figure G-3
Adaptor, Brass
(Gage Holder to Shock Tube)

Vita

John William Frye, Jr. was born [REDACTED]

[REDACTED]
[REDACTED] After graduating from [REDACTED] in 1953, he enrolled at North Carolina State College of Agriculture and Engineering, Raleigh, North Carolina. In May 1958 he graduated with honors, receiving a degree of Bachelor of Mechanical Engineering, Aeronautical Option. A Distinguished Military Graduate of the Air Force R.O.T.C. program, he was commissioned a Second Lieutenant in the USAF Reserves. From college he went to work as an apprentice engineer for Lockheed Aircraft Corporation, Marietta, Georgia. He was subsequently called to active duty in March 1959. Since coming on active duty, he has attended pilots school, Instructor Pilots School, Instrument Instructor Pilots School, Navy Instructor Pilots School, Academic Instructors School, and Programmed Instruction School. When at his assigned base, Laredo AFB, Texas, Capt. Frye performed instructor pilot duties; taught Aerodynamics and Flight Instruments in the classroom; and wrote a text book on flight instruments for the Air Training Command. Capt. Frye also participated as a crew member in a fourteen day simulated Gemini flight conducted at Brooks Aerospace Medical Center, San Antonio, Texas. Capt. Frye was assigned to the Air Force Institute of Technology in June 1964.

PII Redacted

Permanent address: [REDACTED]

This thesis was typed by [REDACTED]

PII Redacted